

AD-A190 433

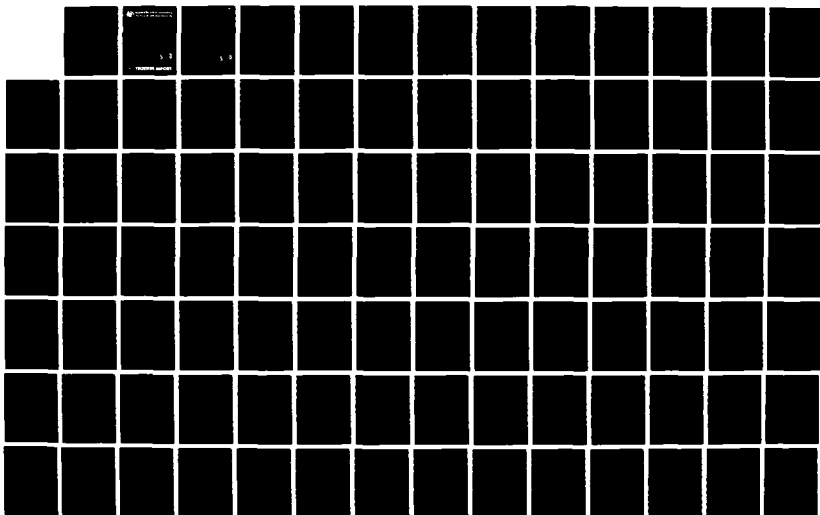
THE SENSITIVITY OF BOUNDARY LAYER INSTABILITY GROWTH
RATES TO COMPLIANT M. (U) PENNSYLVANIA STATE UNIV
UNIVERSITY PARK APPLIED RESEARCH LAB.

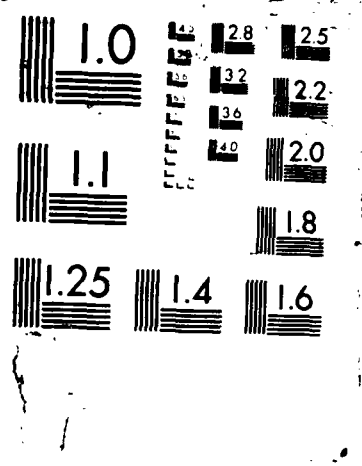
1/2

UNCLASSIFIED

R D JOSLIN ET AL. DEC 87 ARL/PSU/TR-87-014 F/G 20/4

NL







Applied Research Laboratory The Pennsylvania State University

4

AD-A190 433

THE SENSITIVITY OF BOUNDARY LAYER INSTABILITY
GROWTH RATES TO COMPLIANT WALL PROPERTIES

by

R. D. Joslin, P. J. Morris

DTIC
ELECTE
JAN 22 1988
S & D

This document has been approved
for public release and sale; its
distribution is unlimited.

ARLPSU

TECHNICAL REPORT

(2)

The Pennsylvania State University
APPLIED RESEARCH LABORATORY
P.O. Box 30
State College, PA 16804

THE SENSITIVITY OF BOUNDARY LAYER INSTABILITY
GROWTH RATES TO COMPLIANT WALL PROPERTIES

by

R. D. Joslin, P. J. Morris

Technical Report No. TR 87-014
December 1987

Supported by:
Naval Sea Systems Command

L. R. Hettche
Applied Research Laboratory

DTIC
ELECTE
JAN 22 1988
S E D

Approved for public release; distribution unlimited

Unclassified

SECURITY CLASSIFICATION OF THIS PAGE

REPORT DOCUMENTATION PAGE

1a. REPORT SECURITY CLASSIFICATION Unclassified			1b. RESTRICTIVE MARKINGS	
2a. SECURITY CLASSIFICATION AUTHORITY			3. DISTRIBUTION/AVAILABILITY OF REPORT (A) Unlimited	
2b. DECLASSIFICATION/DOWNGRADING SCHEDULE				
4. PERFORMING ORGANIZATION REPORT NUMBER(S) TR-87-014			5. MONITORING ORGANIZATION REPORT NUMBER(S)	
6a. NAME OF PERFORMING ORGANIZATION Applied Research Laboratory The Penna. State University		6b. OFFICE SYMBOL (If applicable) ARL	7a. NAME OF MONITORING ORGANIZATION Naval Sea Systems Command Department of the Navy	
6c. ADDRESS (City, State, and ZIP Code) P. O. Box 30 State College, PA 16804			7b. ADDRESS (City, State, and ZIP Code) Washington, DC 20362	
8a. NAME OF FUNDING/SPONSORING ORGANIZATION Naval Sea Systems Command		8b. OFFICE SYMBOL (If applicable) NAVSEA	9. PROCUREMENT INSTRUMENT IDENTIFICATION NUMBER N-00024-85-C-6041	
8c. ADDRESS (City, State, and ZIP Code) Department of the Navy Washington, DC 20362			10. SOURCE OF FUNDING NUMBERS	
			PROGRAM ELEMENT NO.	PROJECT NO.
			TASK NO.	WORK UNIT ACCESSION NO.
11. TITLE (Include Security Classification) The Sensitivity of Boundary Layer Instability Growth Rates to Compliant Wall Properties				
12. PERSONAL AUTHOR(S) R. D. Joslin and P. J. Morris				
13a. TYPE OF REPORT M.S. Thesis	13b. TIME COVERED FROM _____ TO _____	14. DATE OF REPORT (Year, Month, Day) December 1987	15. PAGE COUNT 100	
16. SUPPLEMENTARY NOTATION				
17. COSATI CODES			18. SUBJECT TERMS (Continue on reverse if necessary and identify by block number)	
FIELD	GROUP	SUB-GROUP	Boundary Layer Dynamics, Flow-induced Surface Instabilities, Laminar Flow, Surface Phenomena, Spatial Stability, Tollmien-Schlichting instability	
19. ABSTRACT (Continue on reverse if necessary and identify by block number)				
<p>A spatial stability analysis is performed for the boundary layer over a non-isotropic compliant surface. A simple mechanical model is used for the surface. Surface properties which may lead to boundary layer stabilization are determined.</p> <p>A spectral approximation is used to obtain a solution of the equations governing the normal velocity component of a small disturbance. The streamwise wavenumber becomes the eigenvalue in the nonlinear eigenvalue problem formed.</p>				
20. DISTRIBUTION/AVAILABILITY OF ABSTRACT <input checked="" type="checkbox"/> UNCLASSIFIED/UNLIMITED <input type="checkbox"/> SAME AS RPT. <input type="checkbox"/> DTIC USERS			21. ABSTRACT SECURITY CLASSIFICATION Unclassified	
22a. NAME OF RESPONSIBLE INDIVIDUAL			22b. TELEPHONE (Include Area Code)	22c. OFFICE SYMBOL

Unclassified

SECURITY CLASSIFICATION OF THIS PAGE

The resulting solution spectrum contains values which indicate the growth rates of the Tollmien-Schlichting and flow-induced surface instabilities. It is shown that the Tollmien-Schlichting instability is most sensitive to changes in the surface properties. Previously it has been suggested that an attempt to stabilize one class of instability tends to destabilize the other class. It is shown that varying the surface properties can reduce the growth rate of the Tollmien-Schlichting instability but has little effect on the flow-induced surface instability.

The surface properties are "optimized" using a minimization algorithm. It is found that appropriate surface properties lead to a decrease in the growth rates of the flow instability. Although this approach may be used it is more expensive computationally than a simple property variation approach.

The simple mechanical model for the compliant surface ~~may be represented by~~ an elastic plate over spring-rigid supports. The functional relationship between the flexural rigidity, thickness, and modulus of elasticity of the plate provides a means to vary the properties and determine the effect on the instabilities. It is found that by keeping the flexural rigidity essentially constant and simultaneously increasing the plate thickness and decreasing the modulus of elasticity a decrease in the growth rate of the Tollmien-Schlichting instability is obtained. Alternatively, by keeping the plate thickness and modulus of elasticity essentially constant and decreasing the flexural rigidity a decrease in the growth rate of the Tollmien-Schlichting instability results. Throughout this analysis little variation is found to occur in the growth rates of the flow-induced surface instability.

Finally, the angle between the rigid support-arm and the horizontal in the mechanical surface model is varied while holding the surface properties constant. It is shown that an angle choice of between 0 and 50 may significantly decrease the growth rate of the Tollmien-Schlichting instability.

Unclassified

SECURITY CLASSIFICATION OF THIS PAGE

ABSTRACT

A spatial stability analysis is performed for the boundary layer over a non-isotropic compliant surface. A simple mechanical model is used for the surface. Surface properties which may lead to boundary layer stabilization are determined.

A spectral approximation is used to obtain a solution of the equations governing the normal velocity component of a small disturbance. The streamwise wavenumber becomes the eigenvalue in the nonlinear eigenvalue problem formed. The resulting solution spectrum contains values which indicate the growth rates of the Tollmien-Schlichting and flow-induced surface instabilities. It is shown that the Tollmien-Schlichting instability is most sensitive to changes in the surface properties. Previously it has been suggested that an attempt to stabilize one class of instability tends to destabilize the other class. It is shown that varying the surface properties can reduce the growth rate of the Tollmien-Schlichting instability but has little effect on the flow-induced surface instability.

The surface properties are "optimized" using a minimization algorithm. It is found that appropriate surface properties lead to a decrease in the growth rates of the flow instability. Although this approach may be used it is more expensive computationally than a simple property variation approach.

The simple mechanical model for the compliant surface may be represented by an elastic plate over spring-rigid supports. The functional relationship between the flexural rigidity, thickness, and modulus of elasticity of the plate provides a means to vary the properties and determine the effect on the instabilities. It is found that by keeping the flexural rigidity essentially constant and simultaneously increasing the plate thickness and decreasing the modulus of elasticity a decrease in the growth rate of the Tollmien-Schlichting instability is obtained. Alternatively, by keeping

the plate thickness and modulus of elasticity essentially constant and decreasing the flexural rigidity a decrease in the growth rate of the Tollmien-Schlichting instability results. Throughout this analysis little variation is found to occur in the growth rates of the flow-induced surface instability.

Finally, the angle between the rigid support-arm and the horizontal in the mechanical surface model is varied while holding the surface properties constant. It is shown that an angle choice of between 0 and 50 may significantly decrease the growth rate of the Tollmien-Schlichting instability.

Accession For	
NTIS GRA&I	<input checked="" type="checkbox"/>
DTIC TAB	<input type="checkbox"/>
Unannounced	<input type="checkbox"/>
Justification	
By	
Distribution/	
Availability Codes	
Dist	Avail and/or Special
A-1	



TABLE OF CONTENTS

	<u>Page</u>
ABSTRACT	iii
LIST OF TABLES	vii
LIST OF FIGURES	ix
LIST OF SYMBOLS	xi
ACKNOWLEDGEMENTS	xiv
 CHAPTER	
1. INTRODUCTION	1
2. PHYSICAL DESCRIPTION AND DERIVATION OF PROBLEM	6
2.1 Introduction	6
2.2 Governing Equations	6
2.3 Compliant Boundary Conditions	10
3. NONLINEAR EIGENVALUE PROBLEM	16
3.1 Introduction	16
3.2 The Orr-Sommerfeld Problem	16
3.3 Solution of the Nonlinear Matrix Eigenvalue Problem	24
3.4 A Model Eigenvalue Problem	29
4. NUMERICAL RESULTS OF EIGENVALUE PROBLEMS	31
4.1 Model Problem	31
4.2 Rigid Wall Case	35
4.3 Compliant Wall Case	40
5. EIGENMODE SENSITIVITY TO BOUNDARY PARAMETERS	48
5.1 Introduction	48
5.2 Model Problem Parameter	48

5.3 Compliant Surface Parameters	50
6. OPTIMIZATION OF BOUNDARY PARAMETERS	57
6.1 Introduction	57
6.2 Minimization Method and Results	57
6.3 Variation Method and Results	61
7. DISCUSSION AND CONCLUSIONS	70
APPENDIX A: CHEBYSHEV SERIES FORMULAE	72
APPENDIX B: BLASIUS SOLUTION REPRESENTED BY A CHEBYSHEV SERIES	79
REFERENCES	82

LIST OF TABLES

<u>Table</u>	<u>Page</u>
4.1 Accuracy of eigenvalues relative to the number of Chebyshev polynomials for the model problem	32
4.2 Values of $R, \bar{\alpha}$, and $\bar{\omega}$ for the neutral curve in the limit as $C_M \rightarrow \infty$ as the compliant surface becomes a rigid plate	36
4.3 Optimum properties of compliant surfaces obtained from Carpenter and Morris [23]	41
4.4 Number of Chebyshev polynomials required for eigenvalue convergence for $R=2240$, $\bar{\omega} = 0.055$, $\theta = 60$ and $B=0.08673 \times 10^{-6}$	42
5.1 Sensitivity of the eigenvalue, $\bar{\alpha}$, to the surface parameter, β , in the model problem with $N=11$ and $\bar{\omega} = 0.25$	51
5.2 Sensitivity of the imaginary part of the wavenumber of TSI to compliant surface property changes	54
5.3 Variation of the sensitivity of the eigenmode to changes in the boundary property, B , with the number of Chebyshev polynomials	55
6.1 Sensitivity of the imaginary part of the wavenumber of FISI to compliant surface property changes for $\theta = 60$ (Carpenter and Morris 1985) and $\bar{\alpha}_i = 0.1462 \times 10^{-3}$	58
6.2 Minimization of instability growth rate by the conjugate gradient approach for $B=0.0773 \times 10^{-6}$, $\rho_m=1000$, and an initial step of 0.05	60
6.3 Sensitivity of the least stable wavenumbers of TSI and FISI to changes in the surface properties: B, E , and b with $K=.059$ and $\rho_m=1000$. (b and E primarily varying)	62

6.4	Sensitivity of the least stable wavenumbers of TSI and FISI to changes in the surface properties: B,E, and b with $K=.059$ and $\rho_m=1000$. (B primarily varying)	65
-----	--	----

LIST OF FIGURES

<u>Figure</u>	<u>Page</u>
2.1	Sketch of a theoretical model representing a non-isotropic compliant surface (Carpenter 1987) 11
3.1	The Blasius solution in the transformed domain 20
4.1	Eigenfunctions of the model problem for $N=5,7,10$; $\bar{\omega}=0.25$; $\bar{\alpha} = .5454$; and $\epsilon = 1.0$ compared with the exact solution 33
4.2	Eigenfunctions of model problem for $N=10$ and $\epsilon_1 = 1.0$, $\epsilon_2 = 1/\sqrt{100}$, $\epsilon_3 = 1/\sqrt{500}$, $\bar{\omega} = 0.25$, $\bar{\alpha} = .5454$ compared with the exact solutions 34
4.3	Curve of neutral stability for the Blasius velocity solution over a rigid surface 37
4.4	Eigenfunction for the rigid surface for $N=15$, $R=998$, $\bar{\omega} = .1122$, and $\bar{\alpha} = (.3086, -.0057)$ 38
4.5	Eigenfunction for the rigid surface for $R=336$, $\bar{\omega} = .1297$, and $\bar{\alpha} = (.3084, .0079)$ 39
4.6	Imaginary part of the complex wavenumber plotted against frequency for $R=2240$ 43
4.7	Real part of the complex wavenumber plotted against frequency for $R=2240$ 44
4.8	Eigenfunctions for the compliant surface with $\theta = 60$, $R=2240$, $\bar{\omega} = 0.055$, $\bar{\alpha} = (.1578, -.0031)$ 46
6.1	Variation of the least stable wavenumber for Tollmien-Schlichting instability versus B and E where E is primarily changed 63

6.2	Variation of the least stable wavenumber for Tollmien-Schlichting instability versus B and b where b is primarily changed	64
6.3	Variation of the least stable wavenumber for Tollmien-Schlichting instability versus B and E where B is primarily changed	66
6.4	Variation of the least stable wavenumber for Tollmien-Schlichting instability versus B and b where B is primarily changed	67
6.5	Variation of the least stable wavenumber for Tollmien-Schlichting instability versus the swivel-arm angle, θ	69

LIST OF SYMBOLS

Chapter 2:

x,y,z	Cartesian coordinate system
t	time variable
U	streamwise velocity in the boundary layer (Blasius solution)
V	transverse velocity in the boundary layer
W	spanwise velocity in the boundary layer
P	pressure in the boundary layer
u'	streamwise velocity perturbation
v'	transverse velocity perturbation
w'	spanwise velocity perturbation
p'	pressure perturbation
u	instantaneous streamwise velocity
v	instantaneous transverse velocity
w	instantaneous spanwise velocity
p	instantaneous pressure
δ^*	displacement thickness
ψ	streamfunction of disturbance
ϕ	amplitude of disturbance
λ	wavelength of disturbance
α	wavenumber(eigenvalue): $= 2\pi/\lambda$
ω	frequency of disturbance
U_∞	maximum freestream velocity
ρ_o	freestream density
$(-)$	nondimensional quantity

(\cdot)	nondimensional disturbance
R	Reynolds number: $= U_{\infty} \delta^* / \nu$
$a(y), b(y)$	nonconstant coefficients of the ordinary differential equation (2.9)
ν	kinematic viscosity
θ	angle between horizontal and rigid-member of surface
ζ	streamwise surface element displacement
η	cross-stream surface element displacement
$\delta\theta$	angular displacement of surface element
ℓ	length of rigid-member support
ρ_m	plate density
b	plate thickness
B	flexural rigidity of plate
E	modulus of elasticity of plate
K	spring stiffness
σ'	viscous normal stress perturbation on plate surface
τ'	viscous shear stress perturbation on plate surface
γ	defined variable: $= \ell \delta\theta$
C_i	nondimensional coefficients of compliant wall properties: $i=M, B, K, T$
μ	viscosity

Chapter 3:

z	transformed computational domain: $\in [-1, +1]$
L	constant used in domain transformation: $z = (y - L) / (y + L)$
m	metric: $m(z) = dz/dy \approx (1 - z)^2 / 2L$
ξ	dummy variable: $\xi = mv'$
T_n	Chebyshev polynomials

e_i	constants of integration: $i=0,1,2,3$
C_i	coefficient matrices: $i=0,1,2,3,4,5$
D_i	lambda matrix: $i=3$ or 5
a	right eigenvector
$\{ \}$	defines vector values
$[]$	defines matrix values
s	constant: $= \bar{\omega}/0.35$
λ	transformed eigenvalue: $= 1/(\bar{\alpha} - s)$
Y	right solvent in factorization
G_n	G-polynomials in Traub iteration
Γ_i	coefficient matrices of G_n -polynomial: $i=1,2,3,4,5,6$
ϕ	model problem function
ϵ	stiffness parameter in model problem: $\sim R^{-1/2}$

Chapter 5:

β	boundary parameter in model problem
a^*	left eigenvector
$()^H$	complex conjugate transpose

ACKNOWLEDGEMENTS

The author is deeply grateful to his advisor, Dr. Philip J. Morris, for providing the guidance, support, and patience necessary throughout the work which is here presented.

Special thanks go to Dr. William W. Hagar of the Mathematics Department at Penn State for the use of his minimization routine, which was very reliable and provided a much needed tool in this analysis. Also, special thanks go to Dr. Goong Chen, formerly of the Mathematics Department at Penn State, for his insights on the characteristics of the spectral method approximation.

This project was possible through the support of the Naval Sea Systems Command and the Applied Research Laboratory Exploratory and Foundational Research Program under NAVSEA N0024-85-C-6041.

CHAPTER 1

INTRODUCTION

This thesis is devoted to identifying non-isotropic compliant surface properties which produce a delay in the transition to turbulence for hydrodynamic applications. This involves using a simple mechanical model for the surface. A disturbance is introduced in the boundary layer in the form of a travelling wave. The streamwise wavenumber of the disturbance becomes the eigenvalue for the nonlinear eigenvalue problem formed. A measure of the instability growth rates is found in the solution spectrum. While the surface properties are varied the least damped wavenumber is tracked to indicate the effect felt by the instabilities. It may be shown that a proper combination of surface properties can lead to boundary layer stabilization.

The transition of boundary layers from laminar to turbulent is due to instabilities that develop in the boundary layer. For low Reynolds number flows, the viscosity is dominant and provides a means to damp-out the instability. As the Reynolds number increases the natural damping becomes insufficient to maintain laminar flow. Waves buildup and eventually turn turbulent. With the onset of turbulence the boundary layer thickens and drag and noise levels increase. In order to delay this effect it is desirable to introduce a passive, "artificial" damping mechanism. This may be accomplished by modifying the surface in contact with the boundary layer.

A major incentive for using a surface other than a rigid wall was brought about by experiments performed by Kramer [1,2] in 1960. By using a rubber coating on a rigid plate, he obtained drag reductions. From his experiments, he concluded: (1) the surface induced artificial damping is a means for boundary layer stabilization; (2) the dimensions and properties of the elastic coating for an average

Reynolds number and speed may be obtained through a simplified theory of distributed damping; (3) up to a 60 percent drag reduction was realized for the coated surface compared to an uncoated identically shaped model; (4) laminar recovery is possible behind surface imperfections which would normally lead to transition; (5) no performance losses occurred due to water impurities; and (6) as the Reynolds number increases the effect of damping should increase due to the improved contact between the boundary layer and wetted surface. Much skepticism has mounted in reference to the results of Kramer since experimental duplication has yet to be realized.

Important understandings of the instabilities occurring over a flexible surface have been brought about by the contributions of Benjamin [3]. His classification of disturbances over a flexible surface was due in part to a stability discussion by Lin [4,5,6] for two-dimensional parallel flows and the analysis by Miles [7,8,9,10] on surface wave generation by shear flows. Landahl [11] and Benjamin [12,13] further identify distinct characteristics which separate the modes of instability into three classes: Class A, Class B, and Class C. The Class A instability is realizable in the presence of viscosity and is essentially a Tollmien-Schlichting instability modified by the flexible surface. The waves are associated with a decrease of the total kinetic energy of the fluid and elastic energy of the wall. Dissipation serves to increase the wave amplitude to compensate for the energy loss. The waves are identified as having a speed less than the velocity of the free surface waves as was discussed by Grosch and Salwen [14]. A Class B instability may occur irrespective of the presence of viscosity and is presumed similar to waves induced by wind over water surfaces. Dissipation in the wall tends to stabilize the wave. The instability may be recognized by a speed greater than the free surface wave. And a Class C instability is realized where the effective stiffness of the panel is too low to withstand the pressure

forces induced on the flexible wall. This instability is more commonly referred to as a Kelvin-Helmholtz instability and occurs when conservative hydrodynamic forces cause a unidirectional transfer of energy to the solid.

Grosskreutz [15,16] introduced a new approach in 1971 which focused on the control of boundary layer stabilization by the use of non-isotropic compliant coatings. His experiments show that compliant coatings may lead to an increase or decrease in momentum thickness which corresponds to an increase or decrease in drag, respectively. So depending on the properties of the compliant coating favorable effects may be obtained or adverse effects may become dominant.

Carpenter and Garrad [17,18] sought to remove the skepticism formed with respect to the isotropic, Kramer-type surface and expand on a numerical model representing the surface. They argue that a Kramer surface does have potential for transition delay and the reason skepticism arose was due to deficiencies in the opposing investigations. Also, the classification established by Benjamin was simplified, or reclassified, to the following two instability classes for a boundary layer. These are the Tollmien-Schlichting instability (TSI) and Flow-induced surface instabilities (FISI). The FISI is basically the Class B instability of Benjamin and Landahl. They explain that the Class C instability is not found due to boundary layer effects. In the analysis of viscous substrates, Carpenter and Garrad concluded that a stabilizing effect is found for TSI in the presence of a substrate and where the two modes coalesce viscous substrates reduce the growth rates of instability. The specific effect on boundary layer stabilization by a viscous substrate under a Kramer-type surface was investigated by Carpenter, Gaster and Willis [19]. It was found to reduce the growth rates of the Tollmien-Schlichting instability.

Carpenter [20,21] arrived at optimum surface properties for the isotropic case which resulted in growth rates of instability less than the rigid wall case. Carpenter

[22] for the non-isotropic case identified a range of desirable surface properties. Carpenter and Morris [23] for spatial wave growth and later Carpenter [24] for temporal wave growth observed growth rates of instability for the non-isotropic compliant surface less than the rigid surface. Morris [25] obtained a slightly modified model which enabled a decrease in the nonlinearity of the eigenvalue problem of [23] and [24] from an order of six to five in the eigenvalue parameter. This model is extended in the present discussion to a spatial stability analysis to identify optimal surface properties which may lead to boundary layer stabilization.

The equations governing the stability of flow over a compliant surface are derived in Chapter 2. This results in the Orr-Sommerfeld equation where the dependent variable is the cross-stream velocity component of an infinitesimal disturbance. A simple mechanical model for the non-isotropic compliant surface may be represented by an elastic plate over spring-rigid supports. The model is chosen to mimic the behavior of a compliant coating such as that designed by Grosskreutz. The coating consists of a thin rubber-type material covering stubs of a similiar material and a viscous substrate fluid surrounding the stubs. The equations governing the motion of an element of this plate together with appropriate far field conditions form the necessary boundary conditions to close the problem.

A spectral method approximation is introduced in Chapter 3 as a means of numerical solution. The resulting matrix of equations forms a nonlinear eigenvalue problem of degree five in the eigenvalue parameter. Methods of solution are then discussed. A model problem with a known solution is introduced to verify the accuracy of the numerical methods.

In Chapter 4, the solutions to the eigenvalue problem are discussed for the model problem and rigid wall and compliant wall boundary layer cases. A comparison between the rigid and compliant case is presented along with the effect and

added cost arising due to the addition of compliance.

In Chapter 5, the means of obtaining a measure of the sensitivity of an eigenvalue to surface property changes is presented and an accuracy comparison is made with a finite difference approximation.

In Chapter 6, the methods of surface property optimization are formulated. The effect of surface property selection for boundary layer stabilization is then shown. The results are presented giving a range of property values which may lead to a delay of transition.

CHAPTER 2

PHYSICAL DESCRIPTION AND DERIVATION OF PROBLEM

2.1 Introduction

Theoretical investigations into the initial stages of transition are based on the assumption that laminar flows are affected by small disturbances. For a boundary layer on a solid body, these disturbances may physically be due to wall roughness or irregularities in the external flow. The question to answer is whether the disturbances increase or decay in time and space. If the disturbances decay, the main flow is considered to be stable; alternatively, if the disturbances increase the flow is considered to be unstable and it is argued that this then leads to transition into turbulent flow. In this section the theory of linear stability is developed with the object of determining the flow conditions which may lead to transition.

2.2 Governing Equations

The problem to be addressed is that of a boundary layer over a smooth, solid surface immersed in an incompressible, uniform flow with constant velocity and pressure. The equations governing the flow are the non-linear Navier-Stokes equations

$$\frac{\partial u}{\partial t} + u \frac{\partial u}{\partial x} + v \frac{\partial u}{\partial y} + w \frac{\partial u}{\partial z} = -\frac{1}{\rho} \frac{\partial p}{\partial x} + \nu \left(\frac{\partial^2 u}{\partial x^2} + \frac{\partial^2 u}{\partial y^2} + \frac{\partial^2 u}{\partial z^2} \right) \quad (2.1a)$$

$$\frac{\partial v}{\partial t} + u \frac{\partial v}{\partial x} + v \frac{\partial v}{\partial y} + w \frac{\partial v}{\partial z} = -\frac{1}{\rho} \frac{\partial p}{\partial y} + \nu \left(\frac{\partial^2 v}{\partial x^2} + \frac{\partial^2 v}{\partial y^2} + \frac{\partial^2 v}{\partial z^2} \right) \quad (2.1b)$$

$$\frac{\partial w}{\partial t} + u \frac{\partial w}{\partial x} + v \frac{\partial w}{\partial y} + w \frac{\partial w}{\partial z} = -\frac{1}{\rho} \frac{\partial p}{\partial z} + \nu \left(\frac{\partial^2 w}{\partial x^2} + \frac{\partial^2 w}{\partial y^2} + \frac{\partial^2 w}{\partial z^2} \right) \quad (2.1c)$$

$$\frac{\partial u}{\partial x} + \frac{\partial v}{\partial y} + \frac{\partial w}{\partial z} = 0, \quad (2.2)$$

where u, v, w , and p are instantaneous flow properties. In stability theory of laminar flows an infinitesimal disturbance is introduced on to the laminar flow solution. Hence, the resulting motion has components

$$u(x, y, z, t) = U(x, y, z, t) + u'(x, y, z, t) \quad (2.3a)$$

$$v(x, y, z, t) = V(x, y, z, t) + v'(x, y, z, t) \quad (2.3b)$$

$$w(x, y, z, t) = W(x, y, z, t) + w'(x, y, z, t) \quad (2.3c)$$

$$p(x, y, z, t) = P(x, y, z, t) + p'(x, y, z, t), \quad (2.3d)$$

where u', v', w' and p' are the disturbances and U, V, W and P are the laminar flow solutions. Equations (2.3) are substituted into (2.1) and (2.2). It is assumed that the undisturbed flow is a solution of the Navier-Stokes equations and that nonlinear terms in the disturbance are neglected. The remaining terms result in differential equations governing the disturbance. In boundary layer flows further stipulations may be made which simplify the governing equations. The motion is essentially two-dimensional since Squire [26] showed that the two-dimensional flow analysis is more critical than three-dimensional; the undisturbed streamwise velocity depends on y only (i.e., $U = U(y)$); and the remaining two mean components, V and W , are everywhere zero. These stipulations describe a class of flows known as *parallel flows*. Boundary layer flows may be regarded as a good approximation to a *parallel flow* because the dependence of the velocity, U , in the streamwise x -direction is much smaller in comparison to the cross-stream y -direction. The resulting components of motion (2.3) may be simplified to

$$u = U(x, y) + u'(x, y, t) \quad (2.4a)$$

$$v = v'(x, y, t) \quad (2.4b)$$

$$w = 0 \quad (2.4c)$$

$$p = P(x) + p'(x, y, t). \quad (2.4d)$$

By substituting (2.4) into (2.1) and (2.2), the resulting equations describe the disturbance in a boundary layer.

$$\frac{\partial u'}{\partial t} + U \frac{\partial u'}{\partial x} + v' \frac{dU}{dy} = -\frac{1}{\rho} \frac{\partial p'}{\partial x} + \nu \left[\frac{\partial^2 u'}{\partial x^2} + \frac{\partial^2 u'}{\partial y^2} \right] \quad (2.5a)$$

$$\frac{\partial v'}{\partial t} + U \frac{\partial v'}{\partial x} = -\frac{1}{\rho} \frac{\partial p'}{\partial y} + \nu \left[\frac{\partial^2 v'}{\partial x^2} + \frac{\partial^2 v'}{\partial y^2} \right] \quad (2.5b)$$

$$\frac{\partial u'}{\partial x} + \frac{\partial v'}{\partial y} = 0 \quad (2.5c)$$

It is also assumed that far from the wall in the cross-stream direction the disturbances vanish.

$$u', v', p' \rightarrow 0 \quad \text{as } y \rightarrow \infty \quad (2.6)$$

This assumption is necessary to satisfy the physical condition and is suitable for securing boundary conditions for the resulting boundary-value problem as will later be shown.

The disturbance is assumed to be a wave which propagates in the x -direction. The stream function representing a single oscillation of the disturbance is assumed to be of the form

$$\psi(x, y, t) = U_{\infty} \delta^* \phi(y) e^{i(\alpha x - \omega t)}, \quad (2.7)$$

where the wave-length of the disturbance is $\lambda = 2\pi/\alpha$ and the frequency of the disturbance is ω . The nondimensional distribution, ϕ , is dependent on y only since the

mean flow depends on y only. The components of the velocity perturbation which are obtained from (2.7) may be defined as partial derivatives of the streamfunction and given as

$$\hat{u} = \frac{\partial \psi}{\partial y} = \delta^* \phi'(y) e^{i(\alpha x - \omega t)} \quad (2.8a)$$

$$\hat{v} = - \frac{\partial \psi}{\partial x} = -i\bar{\alpha} \phi e^{i(\alpha x - \omega t)}, \quad (2.8b)$$

where the hat represents nondimensionalized disturbances and primes denote derivatives with respect to y . Eliminating the pressure from (2.5) and substituting (2.8) into (2.5), a fourth-order, ordinary differential equation results for the cross-stream velocity disturbance. This is given by

$$\hat{v}^{(4)} + a(y)\hat{v}'' + b(y)\hat{v} = 0, \quad (2.9)$$

where

$$a(y) = -iR(\bar{\alpha}\bar{U}(y) - \bar{\omega}) - 2\bar{\alpha}^2$$

$$b(y) = iR\bar{\alpha}^2(\bar{\alpha}\bar{U}(y) - \bar{\omega}) + iR\bar{\alpha}\bar{U}''(y) + \bar{\alpha}^4.$$

This equation has nonconstant coefficients and is commonly referred to as the Orr-Sommerfeld equation which is the stability equation for small disturbances in laminar flows. The equation has been nondimensionalized with the boundary layer displacement thickness, δ^* , the free-stream velocity, U_∞ , and density, ρ_o . The Reynolds number is given by

$$R = \frac{U_\infty \delta^*}{\nu}. \quad (2.10)$$

With equation (2.9), four appropriate conditions are required to obtain a solution for the disturbance. From (2.6) where the disturbances vanish as infinity is approached in the cross-stream direction two boundary conditions result.

$$\hat{v}(y), \quad \hat{v}'(y) \rightarrow 0 \quad \text{as} \quad y \rightarrow \infty \quad (2.11)$$

In the section following, the remaining two boundary conditions necessary to solve (2.9) will be obtained. These are the equations describing the disturbance at the compliant surface.

2.3 Compliant Boundary Conditions:

A simple mechanical model for the non-isotropic compliant surface may be obtained from Morris [25]. This is a revised formulation of Carpenter and Morris [23] and Carpenter [24]. The concepts of the model and derivation of the equations of motion for the disturbance at the surface follow and conclude with the desired boundary conditions. The model consists of a thin, elastic plate supported by hinged and sprung rigid members inclined to the horizontal at an angle θ when in equilibrium. A sketch showing the model is given in Figure (2.1). The motion of the surface is treated such that each element of the plate oscillates in a pendulum like motion at the end of its rigid member. In equilibrium, the rigid members are assumed at rest. The distance between each member is assumed smaller than the wave-length of a disturbance normal to the rigid member. An equation of motion for a surface element is desired which satisfies the constraint that the total force acting on the surface by the mechanical forces is equal to the forces caused by the external fluid motion on the surface. Such an equation may be given by

$$\rho_m b \frac{\partial^2(\ell \delta\theta)}{\partial t^2} + B \frac{\partial^4 \eta}{\partial x^4} \cos\theta + K \ell \delta\theta - Eb \frac{\partial^2 \zeta}{\partial x^2} \sin\theta = -\tau' \cos\theta + \sigma' \cos\theta + \tau' \sin\theta, \quad (2.12)$$

where the terms on the left hand side of (2.12) refer to mechanical forces and the terms on the right refer to fluid motion forces due to viscosity and pressure. For the case of an isotropic surface, viscous interaction on the the right side is neglected and $\theta = 0$.

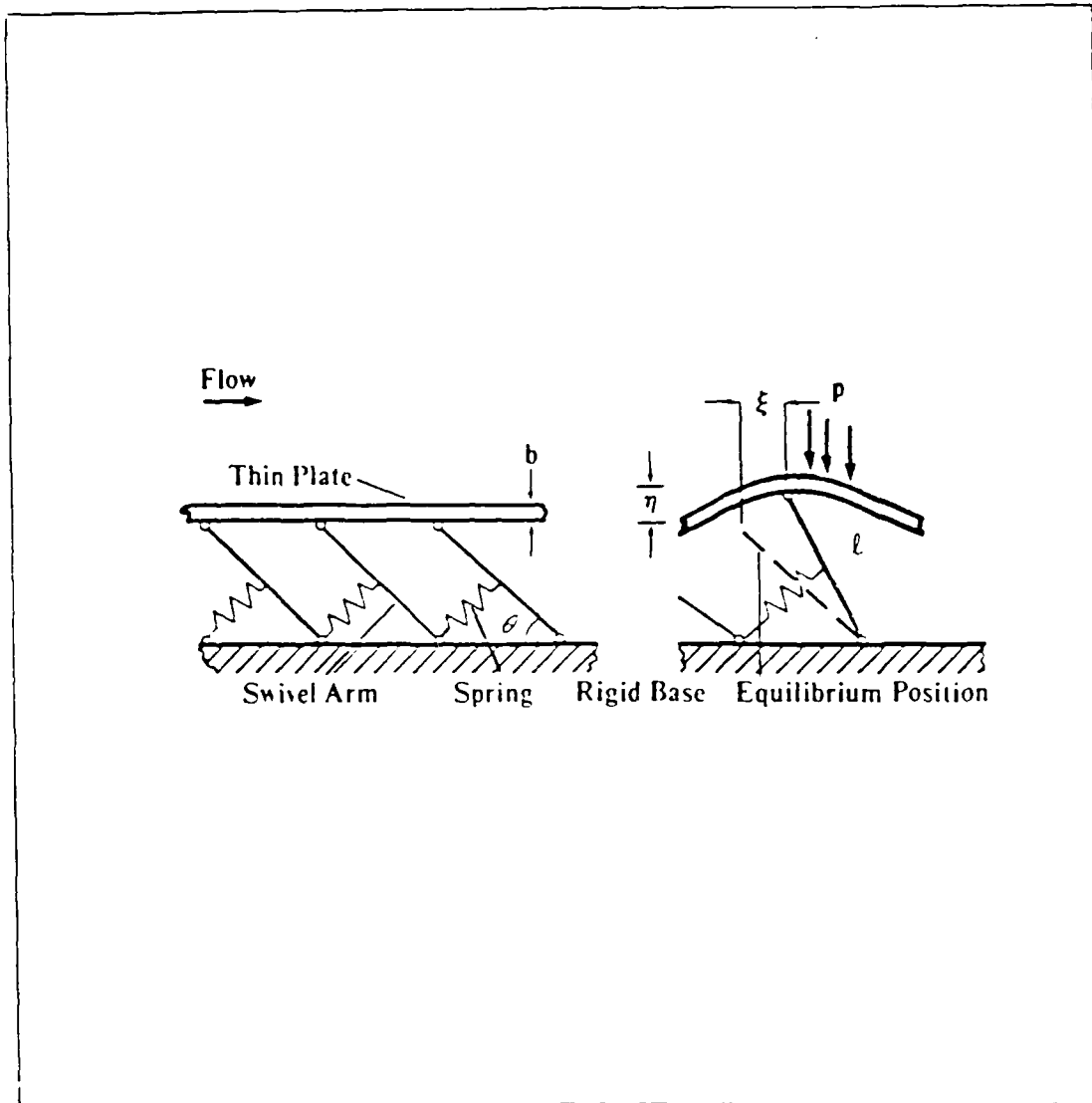


Figure 2.1: Sketch of a theoretical model representing a non-isotropic compliant surface. (Carpenter 1987).

The physical meaning of each term is given respectively as

- (1.) rate of change of momentum of the surface element
- (2.) resistance due to bending stiffness of plate
- (3.) resistance due to spring stiffness
- (4.) tension force induced by relative motion of adjacent rigid members
- (5.) force due to dynamic pressure fluctuations
- (6.) force due to viscous normal stress fluctuations
- (7.) force due to viscous shear stress fluctuations

The variables in (2.12) may be defined as: x and y are the streamwise and cross-stream coordinates; ζ and η correspond to the streamwise and cross-stream surface displacements; $\delta\theta$ is the angular displacement of the element relative to equilibrium; ℓ is the rigid member length; ρ_m and b are the plate density and thickness respectively; B and E are the flexural rigidity and modulus of elasticity of the plate; K is the spring stiffness; and p' , σ' , and τ' are the pressure, viscous normal stress, and viscous shear stress fluctuations on the plate respectively.

The necessary equations of motion for the surface element are coupled by a relationship between the normal and tangential motions (η, ζ) with the angular displacement, $\delta\theta$. This relationship may be given by

$$\zeta = \ell \delta\theta \sin\theta \quad \text{and} \quad \eta = \ell \delta\theta \cos\theta, \quad (2.13)$$

or

$$\ell \delta\theta = \eta / \cos\theta \quad \text{and} \quad \zeta = \eta \tan\theta. \quad (2.14)$$

The normal displacement of the surface is assumed to take the form

$$\eta = \delta^* \bar{\eta} e^{i(\alpha x - \omega t)}. \quad (2.15)$$

The continuity equation for the normal motion at the surface implies

$$\frac{\partial \eta}{\partial t} = \frac{\partial \psi}{\partial x} = v \quad \text{at} \quad y = \eta, \quad (2.16)$$

or linearized: $\bar{\eta}\bar{\omega} = i\hat{v}$.

An alternative form results by letting $\gamma = \ell \delta\theta$ be represented in a similar manner as the normal displacement (2.15). This results in

$$\hat{v} = -i\bar{\omega}\cos\theta\bar{\gamma}. \quad (2.17)$$

The continuity equation for the tangential motion of the surface element implies

$$U + u' = \frac{\partial \zeta}{\partial t} = \frac{\partial \gamma}{\partial t} \sin\theta \quad \text{at} \quad y = \eta, \quad (2.18)$$

or linearized: $U'\eta + u' = \frac{\delta\gamma}{\delta t} \sin\theta$.

The linearization occurs at $y = 0$. Substituting appropriately (2.14), (2.16) and $\hat{u} = -\hat{v}/i\bar{\alpha}$ into (2.18) yields

$$\bar{\alpha}(\bar{U}'(0)\cos\theta + i\bar{\omega}\sin\theta)\hat{v} + \bar{\omega}\cos\theta\hat{v}' = 0. \quad (2.19)$$

Equations (2.12), (2.16), and (2.19) are the resulting equations of motion and boundary conditions. Since the normal and tangential surface motion is coupled one equation may be eliminated algebraically.

Equation (2.12) in nondimensional form appears as

$$\begin{aligned} -C_M\bar{\omega}^2\bar{\gamma} + C_B\bar{\alpha}^4\bar{\gamma}\cos^2\theta + C_K\bar{\gamma} + C_T\bar{\alpha}^2\bar{\gamma}\sin^2\theta \\ = -\hat{p}\cos\theta + \hat{o}\cos\theta + \hat{r}\sin\theta, \end{aligned} \quad (2.20)$$

where

$$C_M = \frac{\rho_m b}{\rho_o \delta^*}, \quad C_B = \frac{B}{\rho_o U_\infty^2 \delta^{*3}}, \quad C_K = \frac{K \delta^*}{\rho_o U_\infty^2}, \quad \text{and} \quad C_T = \frac{Eb}{\rho_o U_\infty^2 \delta^*}.$$

The normal viscous stress perturbation is given by

$$\sigma' = 2\mu \frac{\partial v'}{\partial y}, \quad (2.21a)$$

or nondimensionally

$$\hat{\sigma} = \frac{2}{R} \hat{v}'. \quad (2.21b)$$

The viscous shear stress perturbation is given by

$$\tau' = \mu \left(\frac{\partial v'}{\partial x} + \frac{\partial u'}{\partial y} \right), \quad (2.22a)$$

or nondimensionally

$$\hat{\tau} = \frac{i}{\bar{\alpha} R} (\hat{v}'' + \bar{\alpha}^2 \hat{v}). \quad (2.22b)$$

The pressure perturbation is found from the linearized cross-stream component of the Navier-Stokes equations

$$\bar{\alpha} \bar{\omega} \hat{v}' + \bar{\alpha}^2 \bar{U}' \hat{v} + \bar{\alpha}^2 \bar{U} \hat{v}' = -i \bar{\alpha}^2 \hat{p} - \frac{i}{R} (\bar{\alpha}^2 \hat{v}' - \hat{v}'''), \quad (2.23a)$$

or

$$\hat{p} = -\frac{1}{\bar{\alpha}^2 R} (\hat{v}''' - \bar{\alpha}^2 \hat{v}' + i \bar{\omega} R \hat{v}' + i \bar{\alpha} R \bar{U}' \hat{v}). \quad (2.23b)$$

From the continuity relations the following may be defined

$$\bar{\gamma} = \frac{-i \hat{v}'}{(\bar{\alpha} \bar{U}' \cos \theta + i \bar{\alpha} \bar{\omega} \sin \theta)} \quad (2.24)$$

Substituting (2.21), (2.22), (2.23), and (2.24) into (2.20) and collecting terms with similar powers of $\bar{\alpha}$, the following boundary condition results.

$$\begin{aligned}
 & \bar{\alpha}^5 [C_B \cos^2 \theta \hat{v}'(0)] + \bar{\alpha}^3 [C_T \sin^2 \theta \hat{v}'(0)] \\
 & + \bar{\alpha}^2 [(2\bar{\omega} \sin \theta - 3i\bar{U}'(0) \cos \theta) \frac{\cos \theta}{R} \hat{v}'(0)] \\
 & + \bar{\alpha} [(C_K - \bar{\omega}^2 C_M) \hat{v}'(0) + (\bar{U}'(0) \cos \theta + i\bar{\omega} \sin \theta) \frac{\sin \theta}{R} \hat{v}''(0)] \\
 & + i(\bar{U}'(0) \cos \theta + i\bar{\omega} \sin \theta) \frac{\cos \theta}{R} \hat{v}'''(0) - i\bar{\omega}^2 \sin \theta \cos \theta \hat{v}'(0) = 0 \quad (2.25)
 \end{aligned}$$

The final boundary condition is given by equation (2.19) which is

$$\bar{\alpha}(\bar{U}'(0) \cos \theta + i\bar{\omega} \sin \theta) \hat{v}(0) + \bar{\omega} \cos \theta \hat{v}'(0) = 0.$$

The equations of motion governing the stability of the flow over a non-isotropic compliant surface for the cross-stream velocity component of the disturbance have been derived. The means of obtaining the solution will be described in the next chapter. For convenience, the overbar on U representing the Blasius solution will hereafter be neglected.

CHAPTER 3

NONLINEAR EIGENVALUE PROBLEM

3.1 Introduction

In the previous chapter a detailed analysis was performed to arrive at a mathematical representation of the physical problem, namely the stability analysis of flow over a compliant surface. The present chapter will formulate the equations into a form suitable for obtaining a numerical solution and describe the methods of solution.

3.2 The Orr-Sommerfeld Problem

In hydrodynamic stability theory, the Orr-Sommerfeld equation (2.9) governs the normal velocity component of the disturbance imposed on the flow. The solution will give the characteristic instabilities present for a time or space varying analysis. The problem at hand varies in space and is referred to as a *spatial* stability problem. The wavenumber, $\bar{\alpha}$, is complex and is taken to be the unknown eigenvalue. A negative imaginary part of $\bar{\alpha}$ indicates that the solution is growing in the streamwise direction. This is an indication of an instability growth present in the flow. A zero imaginary part suggests that the solution is neutral. And a positive imaginary part suggests that the solution decays in the streamwise direction. The frequency, $\bar{\omega}$, and Reynolds number, R , are both real and specified. The alternative problem in stability theory which will not be solved in this study is time varying, or *temporal*. In such, $\bar{\alpha}$ and R are both real and specified while the frequency is complex and becomes the unknown eigenvalue of interest. The frequency and wavenumber are related and together form the phase velocity, c , which is defined as $c = \omega / \alpha$.

The problem of boundary layer flow over a flat plate is an eigenvalue problem in $\bar{\alpha}$ and is said to be nonlinear to a degree of four in the eigenparameter. The problem at hand is nonlinear to a degree of five where the added degree of nonlinearity is introduced in the boundary condition (2.25). The nonconstant coefficients result due to the streamwise component of the Blasius velocity profile the solution of which is only known numerically. So the eigenvalue problem must also be solved numerically. The technique used to formulate the numerical approximation was previously used by Bridges and Morris [27,28] and Bridges [29] in the solution of the fourth-order nonlinear eigenvalue problem for the flow over a rigid surface. The reason for such an approach will be made evident.

The domain of the equation is from zero at the surface to infinity in the cross-stream direction. In order to solve the problem numerically, the domain may either be truncated or transformed to some finite domain. Grosch and Orszag [30] have performed a study of this subject and suggest an algebraic transformation

$$z = \frac{y - L}{y + L} \quad \text{and} \quad y = L \cdot \frac{1 + z}{1 - z}, \quad (3.1a, b)$$

where $z \in [-1, +1]$ and $y \in [0, \infty)$. In this analysis a value of $L = 2$ will be used and is suggested as optimum by Bridges for the rigid surface problem. The corresponding metric arrived at is

$$m(z) = \frac{dz}{dy} = \frac{(1 - z)^2}{2L}. \quad (3.2)$$

A far field condition (2.7) in the transformed domain appears as

$$m(z)\hat{v}'(z) = \frac{(1 - z)^2}{2L} \cdot \frac{d\hat{v}(z)}{dz} = 0 \quad \text{as} \quad z \rightarrow 1. \quad (3.3)$$

This introduces an ambiguity as to the value of $\hat{v}'(1)$ since the metric approaches zero as $z \rightarrow 1$. In order to temporarily avoid such a problem, a nondimensional dummy variable, $\xi(z)$, is introduced and defined as

$$\xi = m\hat{v}'. \quad (3.4)$$

Making the appropriate substitutions of (3.2) and (3.4) into (2.9), the Orr-Sommerfeld equation in the transformed domain may be written as

$$m(m(m\xi'))' + ma(z)\xi' + b(z)\hat{v} = 0, \quad (3.5a)$$

where

$$a(z) = -iR(\bar{\alpha}U(z) - \bar{\omega}) - 2\bar{\alpha}^2 \quad (3.5b)$$

$$b(z) = iR\bar{\alpha}^2(\bar{\alpha}U(z) - \bar{\omega}) + i\bar{\alpha}Rm(mU'(z))' + \bar{\alpha}^4 \quad (3.5c)$$

with far field conditions

$$\hat{v}(1) = \xi(1) = 0 \quad (3.6a, b)$$

and compliant boundary conditions

$$\begin{aligned} & \bar{\alpha}^5 \left[C_B \cos^2 \theta \xi(-1) \right] + \bar{\alpha}^3 \left[C_T \sin^2 \theta \xi(-1) \right] \\ & + \bar{\alpha}^2 \left[(2\bar{\omega} \sin \theta + 3iU'(-1) \cos \theta) \frac{\cos \theta}{R} \xi(-1) \right] \\ & + \bar{\alpha} \left[\left(C_K - \bar{\omega}^2 C_M \right) \xi(-1) + (\cos \theta U'(-1) + i\bar{\omega} \sin \theta) \frac{\sin \theta}{R} \xi'(-1) \right] \\ & + \left[i(\cos \theta U'(-1) + i\bar{\omega} \sin \theta) \frac{\cos \theta}{R} \xi''(-1) - i\bar{\omega}^2 \sin \theta \cos \theta \xi(-1) \right] = 0 \end{aligned} \quad (3.6c)$$

and

$$\bar{\alpha}(\cos\theta U'(-1) + i\bar{\omega}\sin\theta)\hat{v}(-1) + \bar{\omega}\cos\theta\xi(-1) = 0, \quad (3.6d)$$

where the nondimensional, constant coefficients were previously defined as

$$C_M = \frac{\rho_m b}{\rho_o \delta^*}, \quad C_B = \frac{B}{\rho_o U_\infty^2 \delta^{*3}}, \quad C_K = \frac{K \delta^*}{\rho_o U_\infty^2}, \quad \text{and} \quad C_T = \frac{Eb}{\rho_o U_\infty^2 \delta^*}.$$

The primes in (3.4)-(3.6) denote derivatives with respect to the transformed variable, z , and $U(z)$ is the Blasius streamwise velocity profile in the transformed domain. A plot of the Blasius profile versus the transformed variable, z , is shown in Figure (3.1). In the limiting case where $C_M \rightarrow \infty$, the compliant problem becomes a rigid wall problem.

A spectral approach known as a finite Chebyshev series expansion is sought for the solution of (3.4)-(3.6). A spectral expansion is an approximation of an unknown function by a series of known functions which satisfy the boundary conditions. Gottlieb and Orszag [31] and Fox and Parker [32] discuss in detail the advantages of such an approximation and give various examples. Gottlieb and Orszag state that a Chebyshev polynomial expansion gives a good representation of functions that undergo rapid changes in narrow boundary layers. One reason is that the polynomials can resolve changes over distances of order n^{-2} where n is the number of Chebyshev series terms retained. Also, for the Chebyshev series expansion the error converges exponentially in comparison to finite difference methods which converge algebraically.

With this in mind, the Chebyshev series expansion for the disturbance in equations (3.4)-(3.6) may be given by

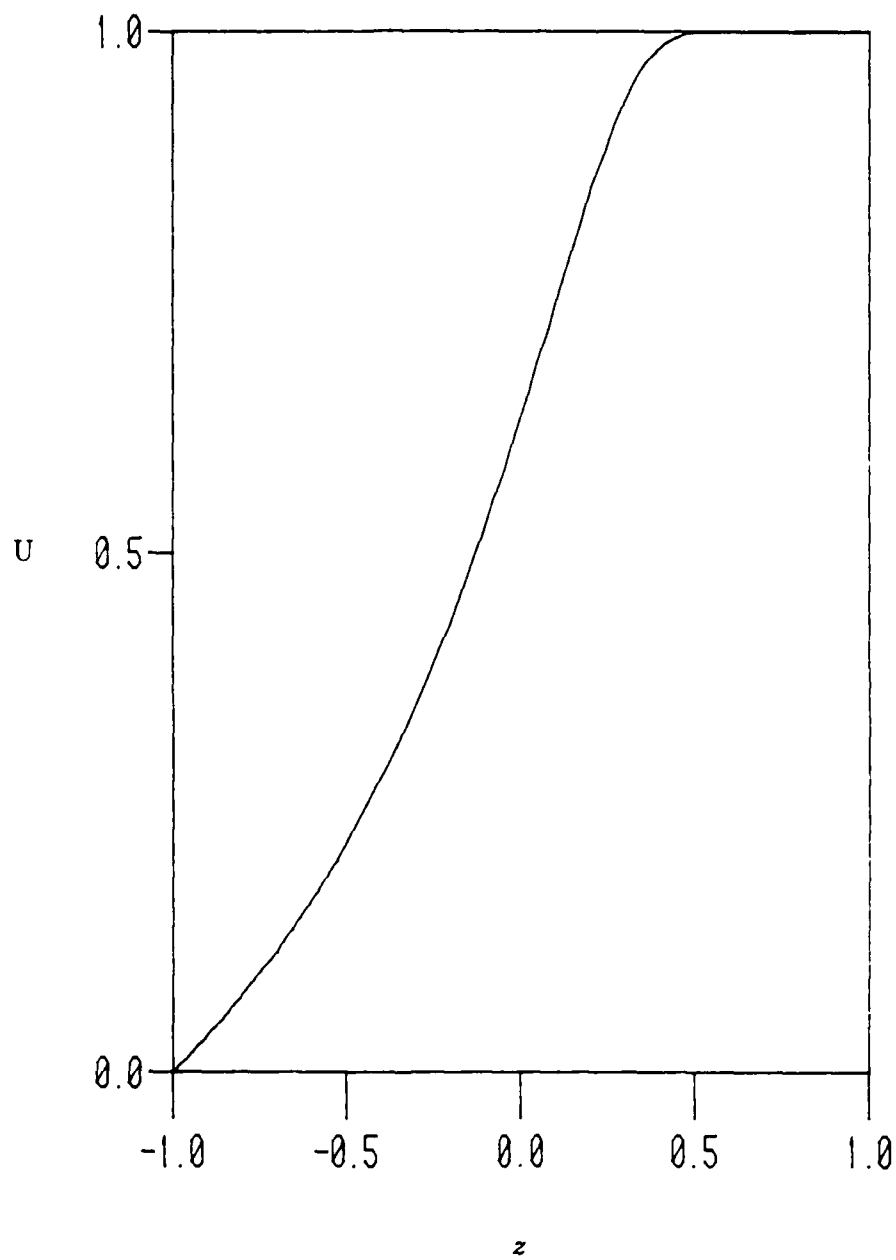


Figure 3.1: The Blasius solution in the transformed domain.

$$\hat{v}(z) = \sum_{n=0}^N {}'v_n T_n(z) \quad (3.7)$$

and

$$\xi(z) = \sum_{n=0}^N {}'\xi_n T_n(z). \quad (3.8)$$

The prime on the summation signifies that the leading term of the series is to be halved. The Blasius velocity profile is expanded in a similiar series.

$$U(z) = \sum_{n=0}^{\infty} {}'u_n T_n(z) \quad (3.9)$$

Details on how a known function may be represented by a Chebyshev series expansion may be found in Appendix A and in Appendix B specifically for the Blasius solution.

Due to the properties of Chebyshev polynomials it is convenient to pose equations (3.4)-(3.6) in integral form. As such, the following equations result.

$$m\hat{v} - \int m'\hat{v} = \int \xi + e_0 \quad (3.10)$$

and

$$\begin{aligned} P_0 \xi + \int P_1 \xi + \int \int P_2 \xi + \int \int \int P_3 \xi + \int \int m a \xi - \int \int \int (ma)' \xi \\ + \int \int \int b v + e_1 + e_2 z + e_3 \frac{z^2}{2} = 0 \end{aligned} \quad (3.11)$$

where $a(z)$ and $b(z)$ are given by (3.5b) and (3.5c), and

$$P_0(z) = m^3 \quad (3.12a)$$

$$P_1(z) = -6m^2m' \quad (3.12b)$$

$$P_2(z) = 7m(m')^2 + 4m^2m'' \quad (3.12c)$$

$$P_3(z) = -(m(mm')')' \quad (3.12d)$$

In connection with a Chebyshev series expansion, the Tau method which was introduced by Lanczos in 1938 will be used to remove the constants of integration. A detailed explanation may be found in [31] and [33], but at present only a brief outline of the method will be presented without proofs.

The series approximation of a function, $\xi(z)$ or $v(z)$, previously introduced in (3.8) and (3.7) has k additional terms added to it where k represents the number of independent boundary constraints that must be applied (i.e., one and three in this particular problem). The resulting approximation is the exact solution to a slightly modified problem. This results in $N + 3$ unknowns for $N + 2$ equations and one boundary constraint for equation (3.10) and $N + 7$ unknown coefficients for $N + 4$ equations and three boundary constraints for equation (3.11). Respectively, the equations involving the coefficients of $T_0(z)$ and $T_0(z), T_1(z)$ and $T_2(z)$ for (3.10) and (3.11) serve to determine the constants of integration only and so may be disregarded for the present analysis. The added "tau" terms need not be explicitly calculated either. The remaining system is composed of N equations with one boundary constraint and $N - 2$ equations with three boundary constraints. The two systems of equations when combined result in a square $N+1$ matrix of equations as will be shown.

Using the Chebyshev product and integral formulae, the series expansions (3.7)-(3.9) and the metric (3.2), represented by the following Chebyshev series

$$m(z) = \frac{3}{2L}T_0(z) - \frac{1}{L}T_1(z) + \frac{1}{4L}T_2(z), \quad (3.13)$$

are substituted into equations (3.10) and (3.11). This results in a set of equations with the vectors of unknown Chebyshev coefficients, $\{\xi\}$ and $\{v\}$. Using the far field condition, $\xi(1) = 0$, with equation (3.10), the following relation is found.

$$\{\xi\} = [T]\{v\} \quad (3.14)$$

$\{\xi\}$ and $\{v\}$ are column vectors containing unknown Chebyshev coefficients and $[T]$ is a square $N + 1$ matrix. The remaining three boundary conditions with equation (3.11) give

$$\left[\sum_{k=0}^5 C_k \bar{\alpha}^{5-k} \right] \{v\} + \left[\sum_{\substack{k=0 \\ k \neq 1}}^5 D_k \bar{\alpha}^{5-k} \right] \{\xi\} = \{0\}, \quad (3.15)$$

where $[C_k]$ and $[D_k]$ are complex square matrices of order $N+1$ which are functions of $\bar{\omega}$, R and the compliant boundary condition properties. The dummy vector, $\{\xi\}$, may be eliminated from (3.15) by the substitution of (3.14). The following nonlinear eigenvalue problem results,

$$[D_5(\bar{\alpha})]\{v\} = \{0\}, \quad (3.16)$$

where

$$D_5(\bar{\alpha}) = C_0 \bar{\alpha}^5 + C_1 \bar{\alpha}^4 + C_2 \bar{\alpha}^3 + C_3 \bar{\alpha}^2 + C_4 \bar{\alpha} + C_5. \quad (3.17)$$

This forms the Chebyshev discretization of the Orr-Sommerfeld equation over a compliant surface.

3.3 Solution of the Nonlinear Matrix Eigenvalue Problem

The eigenvalue problem considered is nonlinear in $\bar{\alpha}$ to the degree of five where the highest degree of nonlinearity is introduced in the boundary condition. The system, $D_5(\bar{\alpha})$, may be referred to as a lambda matrix. Since one boundary condition is independent of $\bar{\alpha}$ it may be eliminated using appropriate column operations; thus, the problem is reduced to N equations and N unknowns, or a system of complex square matrices of order N . For the solution of the lambda matrix, three global methods and one local refinement method will be considered. A global method is global only in the sense that an initial guess for the eigenvalue determination is unnecessary. In a local method an initial guess is required. The global methods are: (1) linearization by a companion matrix, (2) factorization with Bernoulli iteration to obtain a subset of the spectrum, and (3) factorization with Traub iteration to obtain a subset of the spectrum. The local method is a refinement of Newton's method derived by Lancaster [34] for a single eigenvalue.

The companion matrix method has been used for the Orr-Sommerfeld problem by Benney and Orszag [35]. Bridges and Morris [33] and Gohberg, Lancaster and Rodman [36] discuss both the companion matrix method and factorization. From such, the analysis is extended to the larger system at hand. The companion matrix is a linearization of the lambda matrix and therefore is of a larger order. If m is the order of the matrix system, $D_5(\bar{\alpha})$, then the order of the companion matrix is $5m$. When a differential equation is formulated as a matrix problem, it takes on the form of

$$Ax = \lambda Bx \quad (3.19)$$

where λ is the eigenvalue and x represents the eigenvector. Eigenvalue determina-

tion is found by the condition

$$\text{Det}|A - \lambda B| = 0 \quad (3.20)$$

A similar construction for the present problem yields

$$\left\{ \begin{bmatrix} -C_1 & -C_2 & -C_3 & -C_4 & -C_5 \\ I & 0 & 0 & 0 & 0 \\ 0 & I & 0 & 0 & 0 \\ 0 & 0 & I & 0 & 0 \\ 0 & 0 & 0 & I & 0 \end{bmatrix} - \bar{\alpha} \begin{bmatrix} C_o & 0 & 0 & 0 & 0 \\ 0 & I & 0 & 0 & 0 \\ 0 & 0 & I & 0 & 0 \\ 0 & 0 & 0 & I & 0 \\ 0 & 0 & 0 & 0 & I \end{bmatrix} \right\} \begin{Bmatrix} \bar{\alpha}^4 a \\ \bar{\alpha}^3 a \\ \bar{\alpha}^2 a \\ \bar{\alpha} a \\ a \end{Bmatrix} = \{0\}. \quad (3.21)$$

Referring to (3.20), if B is invertible a more efficient and equivalent form is

$$\text{Det}|B^{-1}A - \lambda I| = 0. \quad (3.22)$$

The leading coefficient matrix, $[C_o]$, is singular since the only entries are introduced in the compliant boundary condition as

$$C_o = \begin{pmatrix} 0 & 0 & \dots & 0 \\ 0 & 0 & \dots & 0 \\ \vdots & \vdots & \ddots & \vdots \\ 0 & 0 & \dots & 0 \\ a_{N-1,0} & a_{N-1,1} & \dots & a_{N-1,N} \\ 0 & 0 & \dots & 0 \end{pmatrix}. \quad (3.23)$$

To remove the singularity in $[C_o]$ an algebraic transformation is introduced

$$\lambda = \frac{1}{\bar{\alpha} - s}, \quad (3.24)$$

where s is a real constant taken in this analysis to be $(\bar{\omega}/0.35)$. The problem may now be cast in the form of (3.22) giving

$$A = \begin{pmatrix} -C_o^{-1}C_1 & -C_o^{-1}C_2 & -C_o^{-1}C_3 & -C_o^{-1}C_4 & -C_o^{-1}C_5 \\ I & 0 & 0 & 0 & 0 \\ 0 & I & 0 & 0 & 0 \\ 0 & 0 & I & 0 & 0 \\ 0 & 0 & 0 & I & 0 \end{pmatrix}. \quad (3.25)$$

The eigenvalues of (3.25) may be obtained using the efficient QR algorithm.

The second method is derived by a matrix equivalent to synthetic division to compute the dominant solvent. After applying the algebraic transformation (3.25), the following results

$$D_5(\lambda) = \{Q_4(\lambda)\}(\lambda I - Y) + R_r, \quad (3.26)$$

where

$$\begin{aligned} Q_4(\lambda) = & C_o\lambda^4 + (C_oY + C_1)\lambda^3 + (C_oY^2 + C_1Y + C_2)\lambda^2 \\ & + (C_oY^3 + C_1Y^2 + C_2Y + C_3)\lambda \\ & + (C_oY^4 + C_1Y^3 + C_2Y^2 + C_3Y + C_4) \end{aligned}$$

and is considered to be the right quotient and R_r is the right remainder of the division of $D_5(\lambda)$ by $(\lambda I - Y)$. For $(\lambda I - Y)$ to be a factor of $D_5(\lambda)$, the remainder, R_r , must be set to zero. This is given by

$$R_r = C_oY^5 + C_1Y^4 + C_2Y^3 + C_3Y^2 + C_4Y + C_5 = 0. \quad (3.27)$$

The square matrix, Y , is referred to as the right solvent. The Bernoulli iteration method will be incorporated to solve the matrix polynomial (3.27). For such we seek the dominant solvent which may be obtained from the iteration formula

$$Y_{t+1} = -C_o^{-1}(C_1 + (C_2 + (C_3 + (C_4 + C_5Y_{t-3}^{-1})Y_{t-2}^{-1})Y_{t-1}^{-1})Y_t^{-1}). \quad (3.28)$$

where $Y_0 = Y_1 = Y_2 = Y_3 = 0$ and $Y_4 = -C_0^{-1}C_1$.

Upon convergence, the eigenvalues are obtained by using the QR algorithm.

The final global method to be considered was developed by Dennis, Traub and Weber [37] to compute a dominant solvent. The algorithm is a generalization of an algorithm for scalar polynomials by Traub [38]. The method was discussed by Morris [25] for the compliant problem approaching the limiting case of the rigid wall problem. The method consists of two iterative steps. The first consists of constructing the equivalent of the G-polynomials.

$$G_0(Y) = I \quad (3.29a)$$

$$G_{n+1}(Y) = G_n(Y)Y - \Gamma_1^{(n)}D_5(Y), \quad (3.29b)$$

where

$$G_n(Y) = \Gamma_1^{(n)}Y^5 + \Gamma_2^{(n)}Y^4 + \Gamma_3^{(n)}Y^3 + \Gamma_4^{(n)}Y^2 + \Gamma_5^{(n)}Y + \Gamma_6^{(n)}. \quad (3.29c)$$

The second stage is given by

$$Y_0 = (\Gamma_1^{(L)})(\Gamma_1^{(L-1)})^{-1} \quad (3.30a)$$

and

$$Y_{i+1} = G_L(Y_i)G_{L-1}^{-1}(Y_i) \quad (3.30b)$$

where L is the final G-polynomial built-up. The first stage of the algorithm is equivalent to the Bernoulli iteration. The second stage is only linearly convergent, but the asymptotic error constant may be made as small as desired by increasing the number of iterations of the first stage. A subset of the eigenvalue spectrum may be obtained by using the QR algorithm.

The final method to be considered is a locally convergent algorithm which requires a sufficiently good initial guess for the refinement of a single eigenvalue. The local scheme is a refinement of Newton's method and has quadratic convergence. The method is attributed to Lancaster [34] and an example of its implementation may be found in Bridges and Morris [33]. The iterative formula is given by

$$\bar{\alpha}_{i+1} = \bar{\alpha}_i - 2f(\bar{\alpha}_i)/\{[f(\bar{\alpha}_i)]^2 - f^{(1)}(\bar{\alpha}_i)\}, \quad \text{for } i = 0, 1, 2, \dots \quad (3.31a)$$

where

$$f(\bar{\alpha}_i) = T_r\{D^{-1}(\bar{\alpha}_i)D^{(1)}(\bar{\alpha}_i)\} \quad (3.31b)$$

and

$$f^{(1)}(\bar{\alpha}_i) = T_r\{D^{-1}(\bar{\alpha}_i)D^{(2)}(\bar{\alpha}_i) - [D^{-1}(\bar{\alpha}_i)D^{(1)}(\bar{\alpha}_i)]^2\}. \quad (3.31c)$$

$T_r\{s\}$ denotes the trace of matrix $[s]$, D^{-1} is the inverse of D and $D^{(i)}$ denotes the i th derivative of D with respect to $\bar{\alpha}$. It should be noted that only one matrix inverse is required. Also, as will be discussed in a later chapter, the eigenvectors necessary for the surface property optimization may be conveniently computed as an offshoot of this method making use of the matrix operations already performed.

This concludes the outline of methods considered for eigenvalue determination. Actual global method comparisons for accuracy and efficiency were not in the main context of this investigation. The global schemes are necessary to determine a good initial guess for the least damped eigenvalues for TSI and FISI to be refined in the more efficient local method. The sensitivity of the eigenmodes to changes in the surface properties may then be performed, followed by the optimization of the surface properties. With respect to comparisons and applications, reference may be made to Bridges and Morris [33] and Morris [25].

3.4 A Model Eigenvalue Problem

When investigating a complex problem requiring numerical techniques as a means to obtaining a solution, it is advantageous to devise a model problem with an exact solution which captures as many of the characteristics of the physical problem of interest as possible. One chooses a model problem such that the numerical solution may be compared with the known exact solution. The compliant surface problem has many identifiable characteristics most of which may be incorporated in the model.

The model boundary value problem is given by

$$\epsilon \phi'' - 2\bar{\alpha}\bar{\omega}\phi' + \bar{\alpha}^2\phi = 0 \quad (3.32a)$$

with boundary conditions

$$\phi(1) = 0 \quad (3.32b)$$

$$\bar{\alpha}^3\phi(-1) + \phi'(-1) = 0, \quad (3.32c)$$

where the primes represent derivatives with respect to $z \in [-1, +1]$. The eigenvalue, $\bar{\alpha}$, enters the boundary condition at a higher power than in the differential equation which is similar to the physical problem. A stiffness parameter, ϵ , which may be thought of as $R^{-1/2}$, multiplies the highest derivative so as to simulate the viscous terms in the physical problem.

The exact solution of (3.32) is given by

$$\phi(z) = (e^{\gamma_2 z} + (\bar{\alpha}^3 + \gamma_2)e^{-\gamma_2 z}) / (e^{\gamma_2 z} + (\bar{\alpha}^3 + \gamma_3)e^{-\gamma_2 z}) \quad (3.33)$$

with

$$(\bar{\alpha}^3 + \gamma_2)e^{\gamma_1} - (\bar{\alpha}^3 + \gamma_3)e^{-\gamma_1} = 0 \quad (3.34)$$

and

$$\begin{aligned}\gamma_1 &= \frac{2\bar{\alpha}}{\epsilon} \sqrt{\bar{\omega}^2 - \epsilon} \\ \gamma_2 &= \frac{\bar{\alpha}\bar{\omega}}{\epsilon} - \gamma_1/2 \\ \gamma_3 &= \frac{\bar{\alpha}\bar{\omega}}{\epsilon} + \gamma_1/2.\end{aligned}\tag{3.35}$$

For a numerical solution the equation may be put in integral form, or

$$\epsilon\phi - 2\bar{\alpha}\bar{\omega} \int \phi + \bar{\alpha}^2 \int \int \phi + e_0 + e_1 z = 0.\tag{3.36}$$

The function is approximated by a finite Chebyshev series

$$\phi(z) = \sum_{n=0}^N \phi_n T_n(z).\tag{3.37}$$

By substituting (3.37) into (3.36) and incorporating the Tau method, the problem may be cast into a lambda matrix which is of order three in the eigenvalue and given by

$$D_3(\bar{\alpha}) = C_0 \bar{\alpha}^3 + C_1 \bar{\alpha}^2 + C_2 \bar{\alpha} + C_3,\tag{3.38}$$

where $[C_i]$ are complex square matrices of order $N+1$. The leading coefficient matrix, $[C_0]$, is singular so transformation (3.24) is applied. The methods discussed in the previous section apply in a similar manner to that of the physical problem.

The stage has now been set for solving the problem at hand and the methods of solution for the nonlinear eigenvalue problems have been described. The accuracy of the eigenvalues and eigenfunction for a given number of Chebyshev polynomials will be tested for the compliant wall, the rigid wall, and the model problem in the next chapter.

CHAPTER 4

NUMERICAL RESULTS OF EIGENVALUE PROBLEMS

4.1 Model Problem

As was mentioned in the previous chapter, a model boundary-value problem with characteristics similar to the physical problem is used to test the numerical methods. The global methods of solution were discussed in the previous chapter and results from each method are given in Table (4.1) for $\epsilon = 1.0$ and $\bar{\omega} = 0.25$. As is shown, for a small number of Chebyshev polynomials the methods give a comparatively similar accuracy for the given number of iterations. The Bernoulli and Traub iteration methods result in only a subset of the eigenvalue spectrum. As can be seen the third eigenvalue is undetected by these methods for $N=5$. Since only a sufficiently good initial guess is required for an eigenvalue, little else will be needed in the form of demonstration and comparison with respect to the global methods. A more indepth comparison of these methods and the local method may be obtained from Morris [25], Bridges and Morris [33], Benney and Orszag [35], and Dennis, Traub and Weber [37].

The corresponding eigenfunction is obtained for the smallest eigenvalue in Table (4.1). It is sufficient at present to view the accuracy of the method for a given number of Chebyshev polynomials (N) and an imposed stiffness (ϵ). In Figure (4.1) a plot for $N=5,7$, and 10 with $\epsilon = 1.0$, shows the eigenfunction to be somewhat independent of the number of polynomials. The numerical solution is essentially indistinguishable from the exact solution. The problem is made stiff by requiring the parameter ϵ to be small. The corresponding eigenfunctions for $N=10$ and $\epsilon = 1, 1/\sqrt{100}$, and $1/\sqrt{500}$ are shown in Figure (4.2). The numerical and exact solutions again prove to be indistinguishable. This provides much encouragement

Table 4.1: Accuracy of eigenvalues relative to the number of Chebyshev polynomials for the model problem. ($\epsilon = 1.0$ and $\bar{\omega} = 0.25$).

linear companion matrix method:

	N=5	N=7	N=10	Exact
α_1	0.54543587	0.54541156	0.54541160	0.54541160
α_2	0.98403404	0.98403205	0.98403009	0.98403009
α_3	1.41189790	1.41193160	1.41191660	1.41191660
α_4	1.76754890	1.76666540	1.76673320	1.76673320

Bernoulli iteration(15):

	N=5	N=7	N=10	Exact
α_1	0.54543587	0.54541156	0.54541160	0.54541160
α_2	0.98408419	0.98402771	0.98407944	0.98403009
α_3		1.41134490	1.41176970	1.41191660
α_4	1.76755180	1.76666740	1.76673320	1.76673320

Traub iteration(5:4):

	N=5	N=7	N=10	Exact
α_1	0.54543587	0.54541156	0.54541160	0.54541160
α_2	0.98399391	0.98403206	0.98402854	0.98403009
α_3		1.41192940	1.4119248	1.41191660
α_4	1.76754910	1.76666540	1.76671350	1.76673320

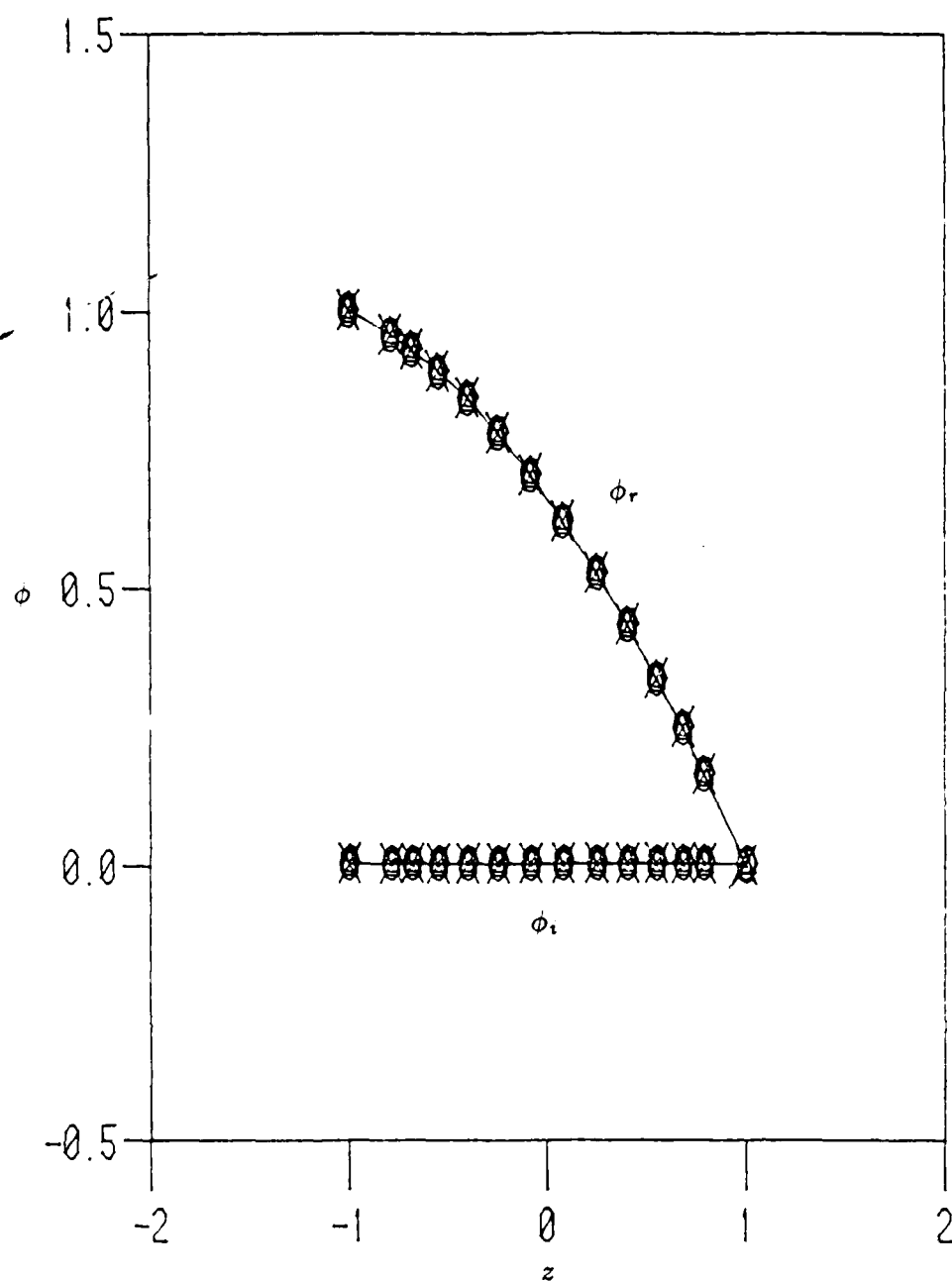


Figure 4.1: Eigenfunctions of the model problem for $N=5,7,10$; $\bar{\omega} = 0.25$; $\bar{\alpha} = .5454$; and $\epsilon = 1.0$ compared with the exact solution.

O - exact X - $N=5$ \wedge - $N=7$ \square - $N=10$.

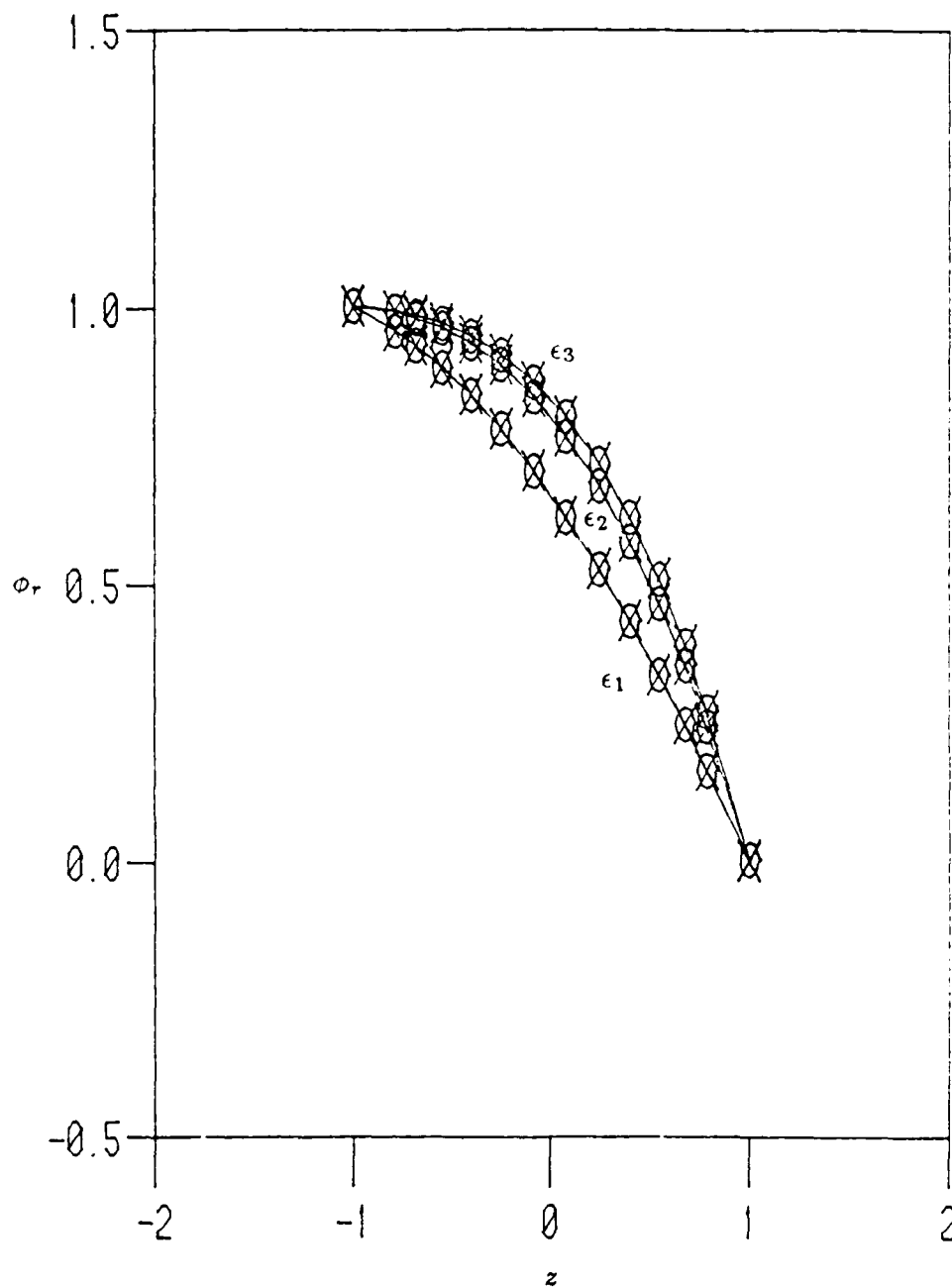


Figure 4.2: Eigenfunctions of model problem for $N=10$ and $\epsilon_1 = 1.0$.
 $\epsilon_2 = 1/\sqrt{100}, \epsilon_3 = 1/\sqrt{500}, \bar{\omega} = 0.25, \bar{\alpha} = .5454$ compared with
the exact solutions. O - numerical X - exact.

for the use of this approach for the physical problem which is stiff.

4.2 Rigid Wall Case

The flow properties used are: the freestream velocity and density are 20 m/s and 1000 kg/m^3 , respectively; the Poisson ratio is 0.5; and the viscosity is $.001002 \text{ kg/ms}$. These are obvious choices for the density and viscosity since water can be found to have a density and viscosity of $1000\text{--}1020 \text{ kg/m}^3$ and $.001002 \text{ kg/ms}$, respectively. The compliant surface model is taken to be a flexible plate. As the mass of the plate is increased, the characteristics of the problem become more similar to that of a rigid, flat surface. The rigid surface is achieved in the limit as the mass coefficient, C_M , approaches infinity. The solutions obtained in this limit should coalesce with published results for the solution of the Blasius velocity profile over a flat plate. A common reference for comparison is the neutral stability curve. For this comparison it is sufficient to use only fifteen Chebyshev polynomials to obtain an adequate accuracy. The results are listed in Table (4.2) and a comparison is made in Figure (4.3) with values from Jordinson [39] and Van Stijn and Van De Vooren [40]. As is expected the results fall on a common curve.

As with the eigenvalue, the normalized eigenfunction comparison must be made with other numerical results since the exact solution is not known. Jordinson [39] referred to the case where $R=998$, $\bar{\omega} = .1122$, and $\bar{\alpha} = (.3086, -.0057)$. Using $N=15$, a comparison results in nearly an exact fit as shown in Figure (4.4). The results begin to deviate slightly as the distance from the wall increases. An observable jump, or step, occurs in Jordinson's analysis which is not found in the present calculations. Since the function is well behaved no physical explanation justifies such a step. And finally a last comparison is made to determine the eigenfunction sensitivity to the number of Chebyshev polynomials. Figure (4.5) is an eigenfunction

Table 4.2: Values of $R, \bar{\alpha}_r$, and $\bar{\omega}$ for the neutral curve in the limit as $C_M \rightarrow \infty$ which as the compliant surface becoming a rigid plate. ($N = 15$).

R	$\bar{\alpha}_r$	$\bar{\omega}$
2200.0	.3095	.1010
1400.0	.3356	.1185
0800.0	.3557	.1368
0520.0	.3014	.1193
0536.5	.2753	.1067
0604.0	.2406	.0893
1364.0	.1450	.0433

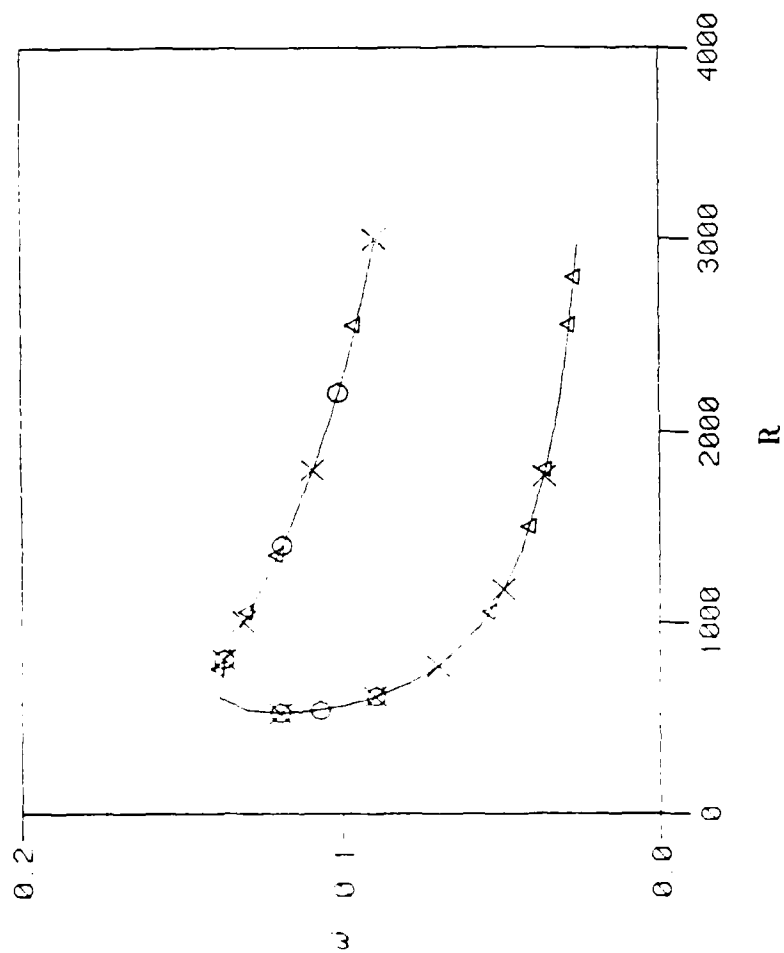


Figure 4.3: Curve of neutral stability for the Blasius velocity solution over a rigid surface. O-present calculations X-Jordinson[39] Δ -Van Stijn and Van De Vooren[40]

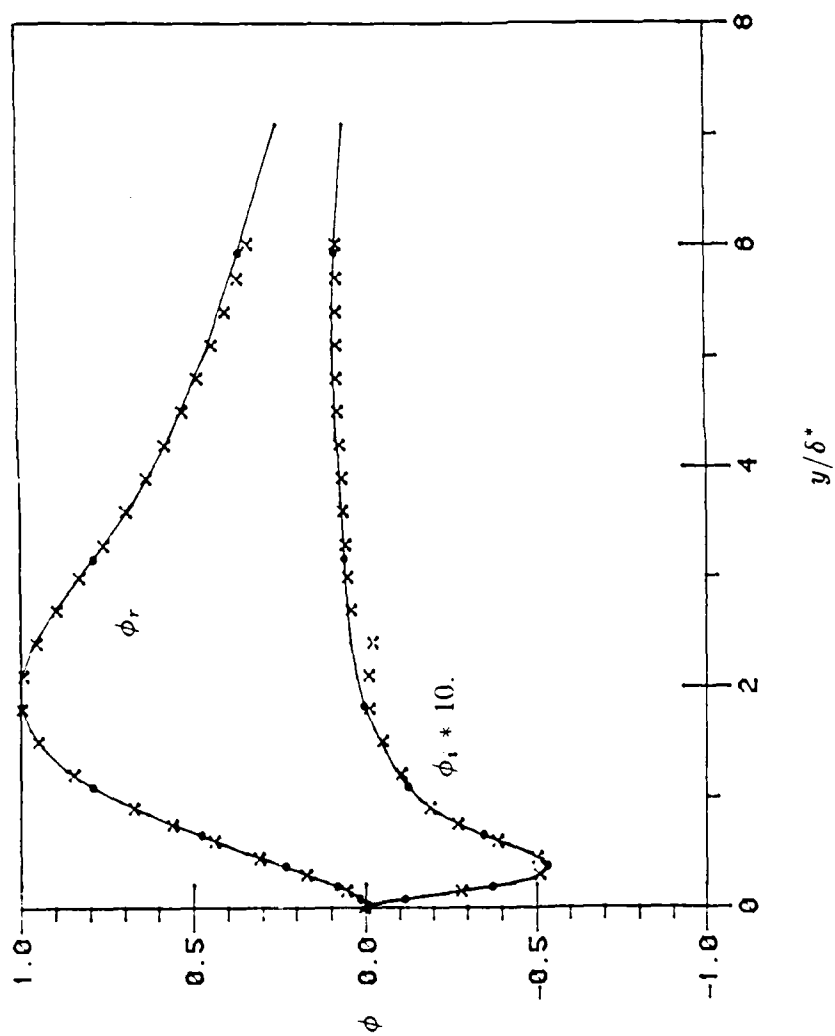


Figure 4.4: Eigenfunction for the rigid surface for $N = 15$, $R = 998$, $\bar{\omega} = .1122$, and $\alpha = (.3086, .0057)$. — present calculations X-Jordinson[39].

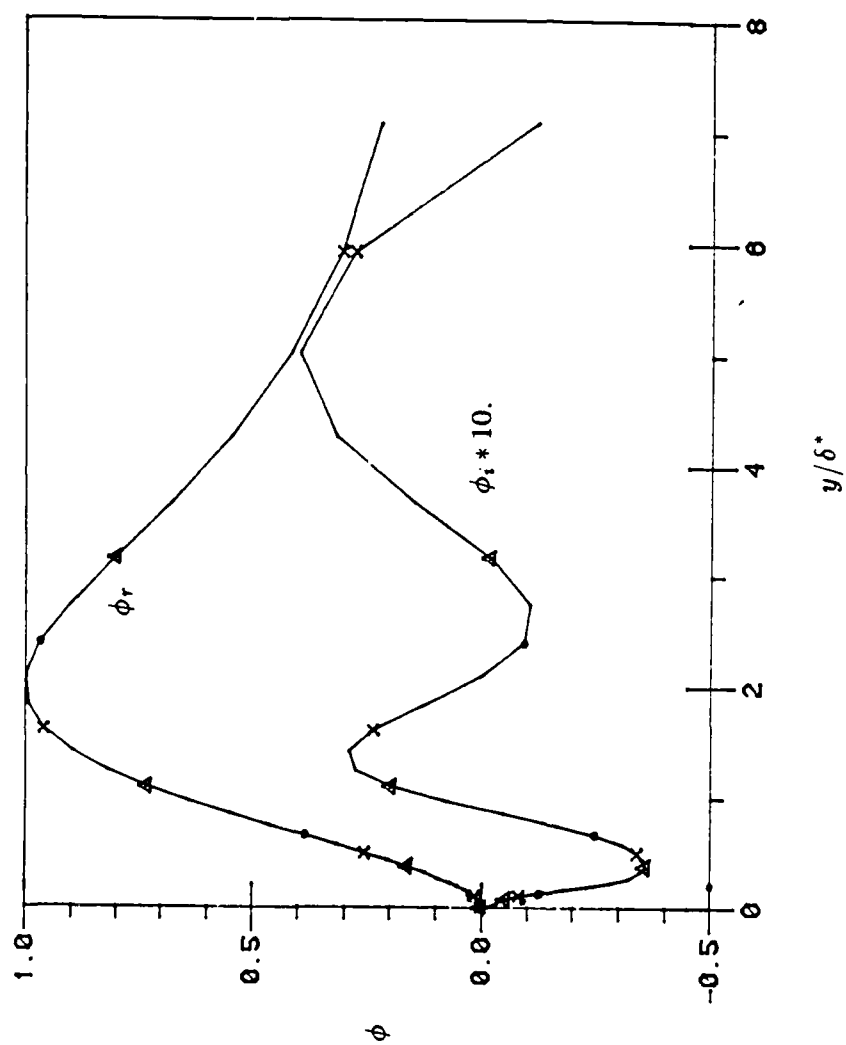


Figure 4.5: Eigenfunction of the rigid surface for $R=336$, $\bar{\omega} = .1297$, and $\bar{\alpha} = (.3084, .0079)$

- Jordinson • - $N=10$ X - $N=15$ Δ - $N=20$.

comparison for $N=10,15$, and 20 with the results by Jordinson corresponding to $R=336$, $\bar{\omega} = .1297$, and $\bar{\alpha} = (.3084, .0079)$. As with the model, the eigenfunctions are relatively independent of the number of Chebyshev polynomials for the rigid wall case to achieve sufficiently accurate solutions.

4.3 Compliant Wall Case

The discussion in this section will primarily be devoted to determining an adequate number of polynomials required for a sufficiently accurate, or converged, solution of eigenvalues and the corresponding eigenfunction. The case that will be examined corresponds to $\theta = 60$ degrees in Table (4.3) obtained from Carpenter and Morris [23] with $R = 2240$, and $\bar{\omega} = 0.055$. Carpenter and Morris chose an appropriate compliant coating density since rubber may have a density of $960\text{-}1300 \text{ kg/m}^3$ [41]. A swivel-arm angle of $\theta = 60$ for the present calculations enables a comparison to be made with the results obtained from the sixth-order model of Carpenter and Morris. The complex wavenumber indicating the onset of instability is of interest in this investigation, so the convergence and accuracy of such are computed. In Table (4.4) the wavenumber is shown to converge, but a large number of polynomials are required for a desired accuracy. The rigid wall case requires only about one-third as many polynomials for a comparable accuracy. Carpenter and Morris chose 48 polynomials for their stability calculations. With this choice the two-digits of accuracy obtained were sufficient for obtaining adequate results. The cost of additional accuracy may be seen in Table (4.4) where a gain of two significant digits results in approximately triple the computational cost.

By looking at the least damped wavenumber for the TSI wave over a frequency variation, the frequency at which the largest growth rate occurs may be determined. Shown in Figures (4.6) and (4.7) are plots of the wavenumber verses the frequency

Table 4.3: Optimum properties of compliant surfaces obtained from Carpenter and Morris [23].

θ (deg)	b (mm)	E (N/mm ²)	K (N/mm ³)	B (Nm)
0	0.7350	1.385	0.354	0.61085×10^{-4}
30	0.4540	0.942	0.191	0.97900×10^{-5}
45	0.2500	0.667	0.119	0.11520×10^{-5}
60	0.1110	0.509	0.059	0.77300×10^{-7}
75	0.0286	0.426	0.016	0.11100×10^{-8}

Table 4.4: Number of Chebyshev polynomials required for eigenvalue convergence for $R=2240$, $\bar{\omega} = 0.055$, $\theta = 60$ and $B=0.08673 \times 10^{-6}$.

N	$\bar{\alpha}$	cpu time(s)
32	.15805932, $-.30840550 \times 10^{-2}$	31.9
40	.15799165, $-.31577908 \times 10^{-2}$	
48	.15781832, $-.31367360 \times 10^{-2}$	
52	.15780772, $-.31282229 \times 10^{-2}$	
56	.15780989, $-.31412738 \times 10^{-2}$	
60	.15781560, $-.31414286 \times 10^{-2}$	
62	.15781491, $-.31393189 \times 10^{-2}$	
65	.15781568, $-.31395635 \times 10^{-2}$	
68	.15781581, $-.31399292 \times 10^{-2}$	
69	.15781518, $-.31392974 \times 10^{-2}$	
72	.15781542, $-.31396316 \times 10^{-2}$	
75	.15781538, $-.31396114 \times 10^{-2}$	109.07

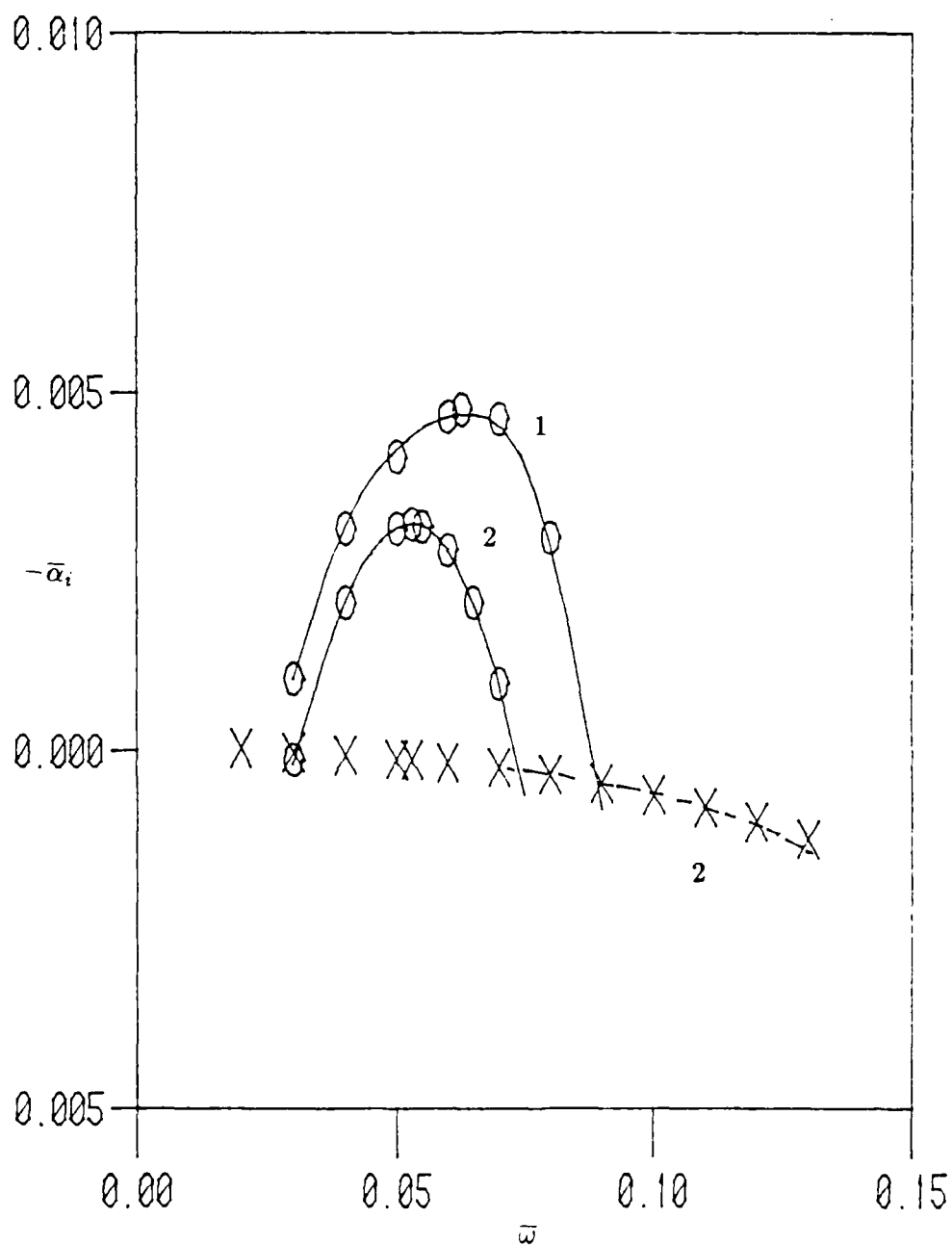


Figure 4.6: Imaginary part of the complex wavenumber plotted against frequency for $R=2240$.

— TSI from [23] O-present calculations

- - Traveling wave-flutter from [23] X-present calculations

1- $\theta = 0$ 2- $\theta = 60$.

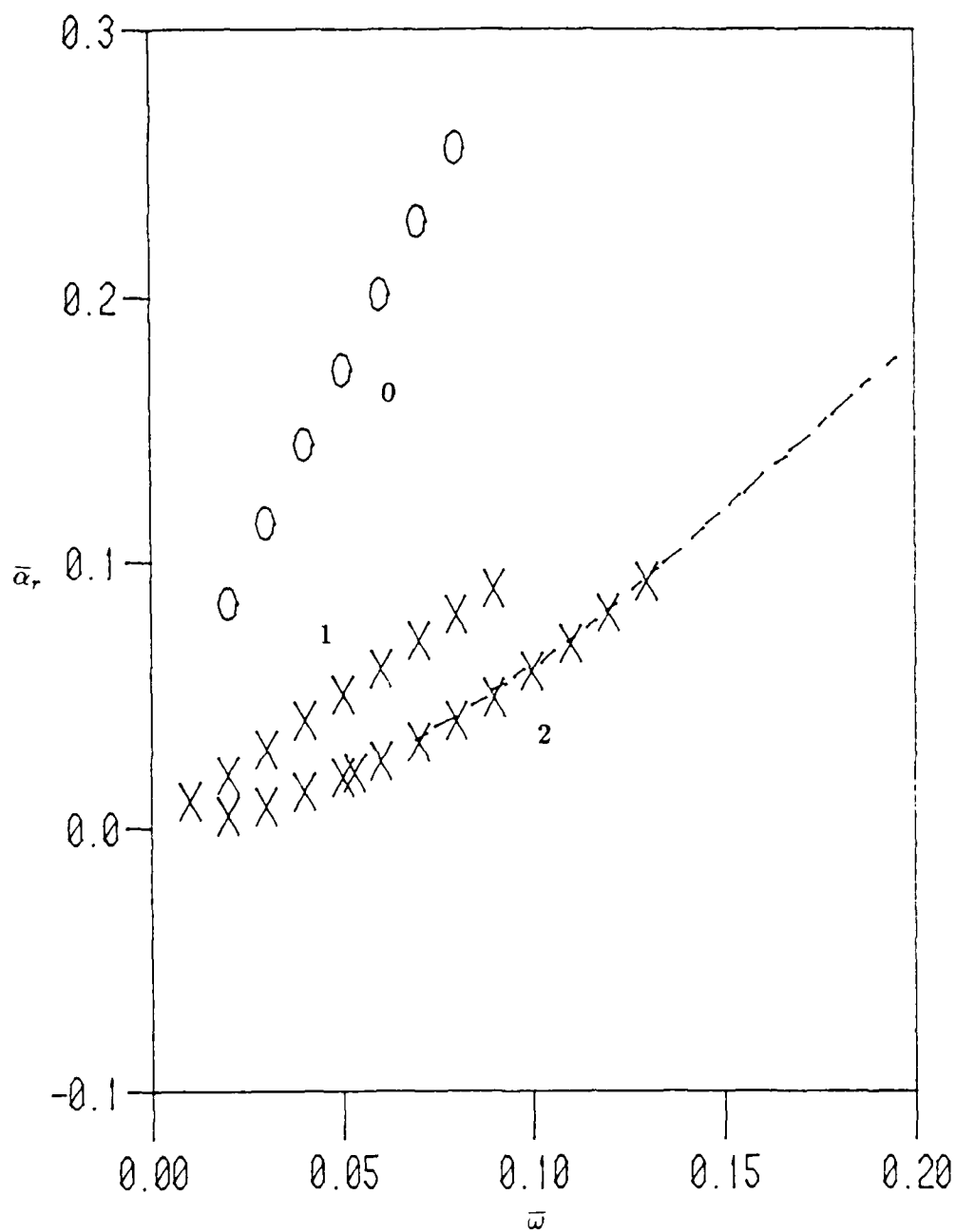


Figure 4.7: Real part of the complex wavenumber plotted against frequency for $R=2240$.

- - Travelling wave-flutter from [23] X-present calculations

O-rigid wall 1- $\theta = 0$ 2- $\theta = 60$

compared with the results obtained by Carpenter and Morris. The results are in agreement. These figures serve two basic functions. First, the revised model formulation by Morris which is being used in the present calculations is shown to be adequate in comparison to the higher order model of [23]. And second, they, along with the surface properties in Table (4.3) form a starting point, or reference point, in the optimization procedure. In conjunction with this, a comparison between these results with a rigid surface makes evident the possibility of delaying transition. At a frequency of 0.055 the compliant surface has a least damped wavenumber of -0.0031 while the rigid surface has a value of -0.01 . This holds for the surface properties of $\theta = 60$. But this investigation seeks to show that by varying the surface properties, reduced growth rates of instability or even complete stabilization of the boundary layer theoretically may be achieved.

A question as to why the large number of Chebyshev polynomials is required arises for the compliant case; one possible answer may be found from analyzing the eigenfunction behavior. The eigenfunctions for $N=10, 24$, and 48 are shown in Figure (4.8) for the least damped wavenumber of TSI. The corresponding results show rather significant differences between the curves near the boundary. If one were to make a comparison of the numerical aspects between the rigid and compliant cases, more insight may be shed on the problem in question. The Chebyshev series coefficients in general have the property that the leading coefficient is the largest in magnitude. The remaining coefficients progressively get smaller as the order of the terms increase. With such the very small, normally insignificant, trailing terms may be neglected to obtain an accurate solution. If this were not the case, then essentially an infinite number of terms would be required for a solution. For the rigid wall case, the smaller terms may be neglected and a relatively accurate solution is obtained. The compliant case behaves in an unconventional manner. The

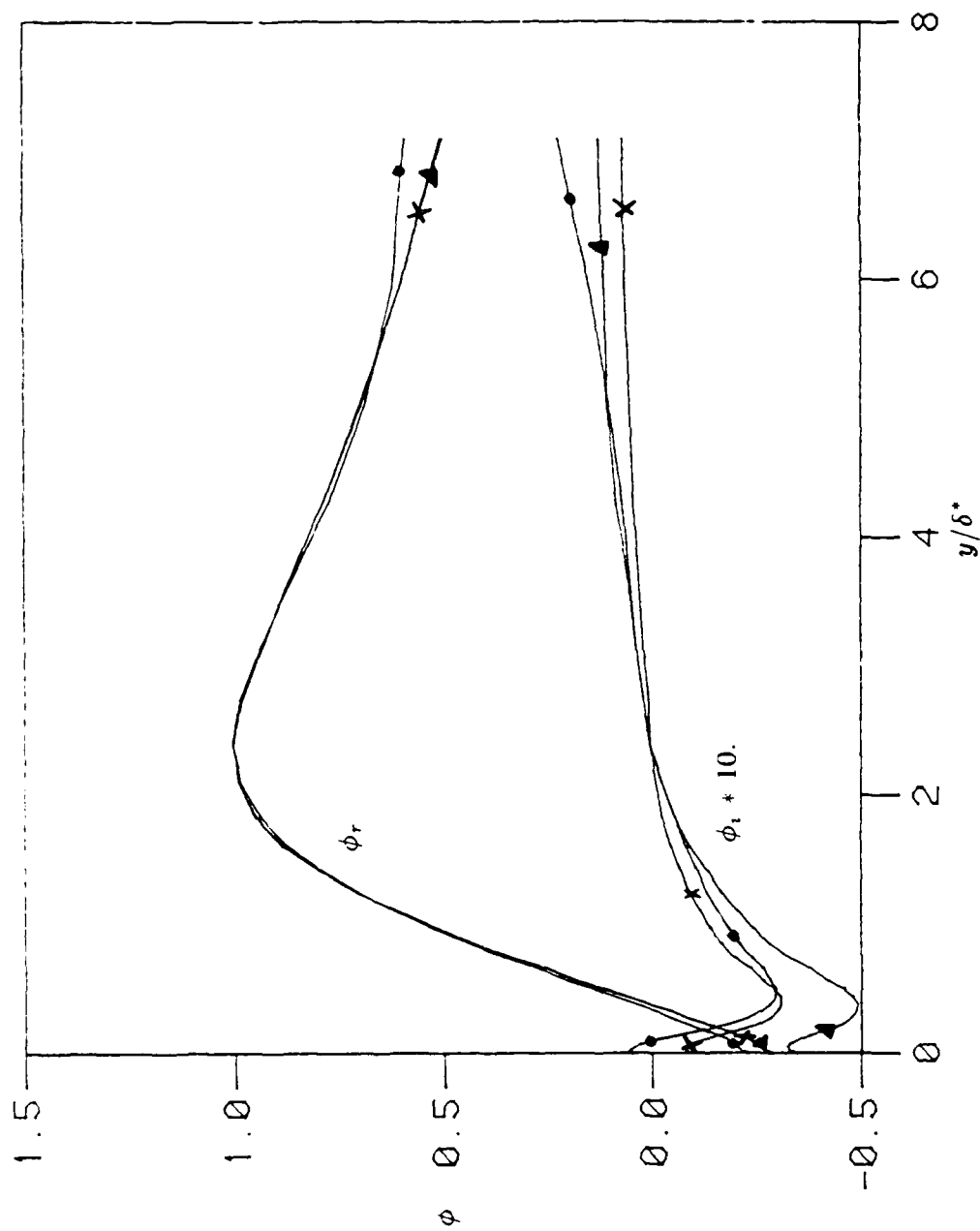


Figure 4.8: Eigenfunctions for the compliant surface with $\theta = 60, R=2240, \omega = 0.055$,

$$\bar{\alpha} = (.1578, -.0031) \quad \bullet - N=10 \quad \times - N=24 \quad \Delta - N=48.$$

leading four or five coefficients decrease in magnitude gradually as is expected; the remaining coefficients drop-off to small values very rapidly and non-uniformly. As before, it might be expected that the smaller trailing terms may be dropped and an accurate solution would be achieved requiring fewer Chebyshev polynomials. This is a somewhat true statement since for $N=10$ a rather crude approximation is achieved. On the other hand, a sufficiently accurate solution requires the very small trailing coefficients to remain a part of the solution. A possible reason for the necessity of the additional terms may lie in the convergence characteristics of the function. It may be possible that although the Euclidean norm of the system becomes small, or converges, this may not be a sufficient convergence criteria. Rather the infinity-norm may not be small.

As a means to reduce the required number of Chebyshev polynomials, stretching factors were implemented to decrease the amount of stiffness in the problem. No reduction in the number of required Chebyshev polynomials resulted. Instead of using Chebyshev polynomials for the series approximation, improved convergence of the series might be realized by using a different polynomial such as the Legendre polynomial. Alternatively, a multi-domain approach may be attempted. The first domain would extend from the compliant surface out in the cross-stream direction a small distance. The outer domain is matched with the inner and proceeds to infinity. The solution of the inner domain would require a larger number of polynomials for an accurate solution as compared to the outer. The idea behind such an approach is that the combined solution may require less polynomials than the single domain problem.

A complete explanation for the behavior of the series approximation for the compliant surface problem is inconclusive at present.

CHAPTER 5

EIGENMODE SENSITIVITY TO BOUNDARY PARAMETERS

5.1 Introduction

An aspect of the surface property optimization is obtaining a technique to determine the changes in the eigenmodes with respect to the boundary parameters. A method which appears to have potential was used by Bridges and Morris [27,33] to determine the frequency of the most unstable eigenvalue will be used here to determine the sensitivity of the least damped eigenmodes to boundary parameter changes. In Chapter 3 it was mentioned that Lancaster's local eigenvalue refinement method could be extended to perform a portion of the optimization procedure. The formulation of the method will be described and tested using the model problem then extended to the physical problem.

5.2 Model Problem Parameter

Since the optimization desired occurs with respect to boundary parameters, a modification is made to the model problem (3.32). A nondimensional surface parameter, β , is introduced giving the modified boundary condition.

$$\beta \bar{\alpha}^3 \phi(-1) + \phi'(-1) = 0 \quad (5.1)$$

The spectral discretization results in

$$[D_3(\bar{\alpha}, \beta)] \{a\} = \{0\}, \quad (5.2)$$

where $\{a\}$ is the right eigenvector and the lambda matrix is given by

$$D_3(\bar{\alpha}, \beta) = C_o \beta \bar{\alpha}^3 + C_1 \bar{\alpha}^2 + C_2 \bar{\alpha} + C_3.$$

Before deriving the necessary relation, an additional vector must be defined and a means of obtaining this vector as well as the right eigenvector must be discussed. This vector may be defined such that

$$\{a^*\}^H [D_3(\bar{\alpha}, \beta)] = \{0\}, \quad (5.3)$$

where $\{a^*\}$ is referred to as the left eigenvector and H denotes the complex conjugate transpose. Relation (5.3) may also be cast in the form

$$[D_3^H(\bar{\alpha}, \beta)] \{a^*\} = \{0\}. \quad (5.4)$$

This has a similar form to (5.2) for the right eigenvector; so a common technique for determining the eigenvectors may be used. To compute a single eigenvector the following inverse iteration is used

$$[D(\bar{\alpha})] \{x^{k+1}\} = \sigma \{x^k\}, \quad (5.5)$$

where σ is a scaling, or normalizing, factor. The procedure converges in two or three iterations using an initial guess of $\{x^0\} = [1, 1, \dots, 1]^T$. The right eigenvector may be conveniently computed using the already formed lambda matrix, $[D]$, from the local method; the left eigenvector may similarly be computed with the inverted lambda matrix, $[D^{-1}]$, from the local method by-way-of the relation $[A^{-1}]^H = [A^H]^{-1}$.

The necessary components for the differentiation have been computed, so the derivation of the sensitivity relations will follow. If the matrix system (5.2) is

differentiated with respect to the boundary parameter, β , the following may be obtained.

$$\frac{\partial \bar{\alpha}}{\partial \beta} [D_3^{(1)}] \{a\} + \frac{\partial [D_3]}{\partial \beta} \{a\} + [D_3] \frac{\partial \{a\}}{\partial \beta} = \{0\} \quad (5.6)$$

By multiplying (5.6) by $\{a^*\}^H$ the last term is eliminated and the result is

$$\frac{\partial \bar{\alpha}}{\partial \beta} = - \frac{\{a^*\}^H (\partial [D_3] / \partial \beta) \{a\}}{\{a^*\}^H [D_3^{(1)}(\bar{\alpha}, \beta)] \{a\}}. \quad (5.7)$$

Recall that the parameter, β , appears only in the leading coefficient matrix, so (5.7) may be given by

$$\frac{\partial \bar{\alpha}}{\partial \beta} = - \frac{\{a^*\}^H [C_o] \bar{\alpha}^3 \{a\}}{\{a^*\}^H [3\beta C_o \bar{\alpha}^2 + 2C_1 \bar{\alpha} + C_2] \{a\}}. \quad (5.8)$$

The matrix $[D_3^{(1)}]$ may also be taken from the local method described in Chapter 3. From (5.8) a means has been obtained to determine the effect of an eigenmode to changing surface parameters, or more specifically, the sensitivity of the least damped wavenumber to surface property variations.

The accuracy of (5.8) may be determined by a comparison of this method with a finite difference approximation. The results in Table (5.1) for $N = 11$ and $\bar{\omega} = 0.25$ show good agreement between the finite difference approximation and the approach of (5.8) for the model problem.

5.3 Compliant Surface Parameters

The formulation for the sensitivity of the eigenmode to a boundary parameter may similarly be applied to the mechanical model representing a compliant surface.

Table 5.1: Sensitivity of the eigenvalue, $\bar{\alpha}$, to the surface parameter, β , in the model problem with $N=11$ and $\bar{\omega} = 0.25$.

R	β	$\bar{\alpha}$	Numerical	F.Diff.	Error
1.	1.00	.5454	$-.8344 \times 10^{-1}$	$-.8492 \times 10^{-1}$	$.17 \times 10^{-3}$
	0.95	.5496	$-.8642 \times 10^{-1}$	$-.8645 \times 10^{-1}$	$.33 \times 10^{-6}$
	0.90	.5540	$-.8960 \times 10^{-1}$	$-.8799 \times 10^{-1}$	$.18 \times 10^{-3}$
100.	1.00	.9451	$-.2756 \times 10^{-1}$	$-.2779 \times 10^{-1}$	$.12 \times 10^{-3}$
	0.95	.9465	$-.2821 \times 10^{-1}$	$-.2822 \times 10^{-1}$	$.16 \times 10^{-5}$
	0.90	.9479	$-.2890 \times 10^{-1}$	$-.2855 \times 10^{-1}$	$.12 \times 10^{-3}$
500.	1.00	.09953	$-.2194 \times 10^{-3}$	$-.2195 \times 10^{-3}$	$.35 \times 10^{-5}$
	0.95	.09954	$-.2196 \times 10^{-3}$	$-.2196 \times 10^{-3}$	$.34 \times 10^{-6}$
	0.90	.09955	$-.2197 \times 10^{-3}$	$-.2197 \times 10^{-3}$	$.29 \times 10^{-5}$

Two basic approaches may be formed. The differentiation may be made with respect to the non-dimensional coefficients or the dimensional physical properties.

The first approach leads to the following relations

$$\frac{\partial \bar{\alpha}}{\partial C_B} = - \frac{\{a^*\}^H [\bar{\alpha}^5 \cos^2 \theta \{\hat{v}'(-1)\}] \{a\}}{\{a^*\}^H [D_5^{(1)}(\bar{\alpha})] \{a\}} \quad (5.9a)$$

$$\frac{\partial \bar{\alpha}}{\partial C_T} = - \frac{\{a^*\}^H [\bar{\alpha}^3 \sin^2 \theta \{\hat{v}'(-1)\}] \{a\}}{\{a^*\}^H [D_5^{(1)}(\bar{\alpha})] \{a\}} \quad (5.9b)$$

$$\frac{\partial \bar{\alpha}}{\partial C_K} = - \frac{\{a^*\}^H [\bar{\alpha} \{\hat{v}'(-1)\}] \{a\}}{\{a^*\}^H [D_5^{(1)}(\bar{\alpha})] \{a\}} \quad (5.9c)$$

$$\frac{\partial \bar{\alpha}}{\partial C_M} = - \frac{\{a^*\}^H [-\bar{\alpha} \omega^2 \{\hat{v}'(-1)\}] \{a\}}{\{a^*\}^H [D_5^{(1)}(\bar{\alpha})] \{a\}} \quad (5.9d)$$

The second approach may be performed in two ways. Either determine the values of (5.9) then multiply the result by an appropriate derivative resulting in

$$\frac{\partial \bar{\alpha}}{\partial C_i} \cdot \frac{\partial C_i}{\partial s} = \frac{\partial \bar{\alpha}}{\partial s}, \quad (5.10)$$

where s is the dimensional surface parameter of interest; or differentiate with respect to the dimensional boundary properties explicitly. This approach yields the following relations

$$\frac{\partial \bar{\alpha}}{\partial b} = - \frac{\{a^*\}^H [(\bar{\alpha}^3 E) / (\rho_o U_\infty^2 \delta^*) - (\bar{\alpha} \omega^2 \rho_m) / (\rho_o \delta^*)] \{\hat{v}'(-1)\} \{a\}}{\{a^*\}^H [D_5^{(1)}(\bar{\alpha})] \{a\}} \quad (5.11a)$$

$$\frac{\delta \bar{\alpha}}{\delta B} = - \frac{\{a^*\}^H [(\bar{\alpha}^5 \cos^2 \theta) / (\rho_o U_\infty^2 \delta^{*3})] \{\hat{v}'(-1)\} \{a\}}{\{a^*\}^H [D_5^{(1)}(\bar{\alpha})] \{a\}} \quad (5.11b)$$

$$\frac{\partial \bar{\alpha}}{\partial E} = - \frac{\{a^*\}^H [(\bar{\alpha}^3 b \sin^2 \theta) / (\rho_o U_\infty^2 \delta^*) \{\hat{v}'(-1)\}] \{a\}}{\{a^*\}^H [D_5^{(1)}(\bar{\alpha})] \{a\}} \quad (5.11c)$$

$$\frac{\partial \bar{\alpha}}{\partial K} = - \frac{\{a^*\}^H [(\bar{\alpha} \delta^*) / (\rho_o U_\infty^2) \{\hat{v}'(-1)\}] \{a\}}{\{a^*\}^H [D_5^{(1)}(\bar{\alpha})] \{a\}} \quad (5.11d)$$

$$\frac{\partial \bar{\alpha}}{\partial \rho_m} = - \frac{\{a^*\}^H [(-\bar{\alpha} \bar{\omega}^2 b) / (\rho_o \delta^*) \{v'(-1)\}] \{a\}}{\{a^*\}^H [D_5^{(1)}(\bar{\alpha})] \{a\}}. \quad (5.11e)$$

Both approaches should render identical results. The reason for giving both approaches is to verify the prospect of performing the analysis with the four nondimensional variables as opposed to the five physical variables. Depending on the scope of the analysis for a given problem using the above differential technique, it may be more practical to use fewer nondimensional variables if possible.

As with the model, the method is shown to be accurate in comparison to finite difference approximations. The results are compared in Table (5.2) with $N = 48$, $\bar{\omega} = 0.055$, $R = 2240$, and the surface properties corresponding to the case where $\theta = 60$ of Carpenter and Morris [23]. A comparison showing the influence of the number of Chebyshev polynomials on the accuracy of the differential is given in Table (5.3). Obviously increasing the number of Chebyshev series terms increases the number of accurate significant digits. To obtain an eigenvalue with two significant digits of accuracy 48 polynomials are required. For the sensitivity with a similar number of polynomials two significant digits of accuracy are retained. This may lead one to conclude that the accuracy of the sensitivity measure is related to the eigenvalue accuracy of interest. So the choice of the number of Chebyshev polynomials required is based on the desired accuracy of the eigenvalue in question.

Up to this point the tools necessary for the optimization procedure have been derived and analyzed. The local eigenvalue refinement method, the eigenvector determination scheme, and the formula relating the sensitivity of eigenmodes to

Table 5.2: Sensitivity of the imaginary part of the wavenumber of TSI to compliant surface parameters. (Approach:1 is equations (5.9) and (5.10) and Approach:2 is equations (5.11)).

s	$\bar{\alpha}_i$	Approach:1 $\partial \bar{\alpha}_i / \partial s$	Approach:2 $\partial \bar{\alpha}_i / \partial s$	F.Diff. $\partial \bar{\alpha}_i / \partial s$
$b(mm)$.11101	-.003133	$- .4534 \times 10^{-1}$	$.4534 \times 10^{-1}$	$- .4539 \times 10^{-1}$
ρ_m 1000.	-.003132	$+ .6250 \times 10^{-6}$	$+ .6250 \times 10^{-6}$	$+ .6258 \times 10^{-6}$
$B(Nmm)$ $.82300 \times 10^{-4}$	-.003140	$- .7464 \times 10^{-1}$	$.7464 \times 10^{-1}$	$.7445 \times 10^{-1}$
$E(N/mm^2)$.509	-.003132	$- .1112 \times 10^{-1}$	$.1112 \times 10^{-1}$	$.1113 \times 10^{-1}$
$K(N/mm^3)$.059	-.003133	$- .5861 \times 10^{-1}$	$.5861 \times 10^{-1}$	$.5868 \times 10^{-1}$

Table 5.3: Variation of the sensitivity of the eigenmode to changes in the boundary property, B , with the number of Chebyshev polynomials. ($B(Nm) = 0.773 \times 10^{-7}$).

N	$\bar{\alpha}$	Numer: $\partial \bar{\alpha} / \partial B$	F.Diff.: $\partial \bar{\alpha} / \partial B$
33	.15804017, -.00293839	213.16244, -78.565489	101.4, -80.12
38	.15757249, -.00295601	217.97623, -73.151999	218.0, -74.39
41	.15774825, -.00295831	216.67877, -75.295445	216.0, -76.20
48	.15781629, -.00313296	215.11468, -74.643011	215.0, -74.72
55	.15781285, -.00314088	214.94787, -74.624582	215.0, -74.64

surface property changes may be linked together to complete this investigation. What remains is the introduction of a minimization procedure for multi-variable optimization problems and the presentation of a simple property variation approach.

CHAPTER 6

OPTIMIZATION OF BOUNDARY PARAMETERS

6.1 Introduction

In the remaining segment of this discussion the importance of the surface property changes on boundary layer stabilization will be shown. Numerical techniques outlined in the previous chapter are utilized to measure the instability growth or decay depending on the surface property variations.

6.2 Minimization Method and Results

In Chapter 5 a means was developed to determine numerically the sensitivity of an eigenvalue to surface property changes. Relatively speaking, this may be considered a gradient. This is verified by a comparison with the finite difference approximation. These gradient measurements are the desired agents needed for the optimization algorithm available.

Many algorithms have been proposed for minimizing a function of multi-variable problems. Gradients are not necessary to obtain the desired results as is explained by Powell [42]; however, many benefits are found in the use of gradients. For instance, the relative influence of each property is made evident in the gradient. In the present investigation, the influence of a property may be found to have a dominant effect on the growth or decay of the instability as opposed to a property having no effect on the instability. This is significant in the present problem for understanding the relative importance of the sensitivity of TSI and FISI waves with the surface property changes. The measure of TSI sensitivity was given in Table (5.2), and the FISI sensitivity measurements are given in Table (6.1). The TSI sensitivity values are one or two orders of magnitude greater than the FISI

Table 6.1: Sensitivity of the imaginary part of the wavenumber of FISI to compliant surface property changes for $\theta = 60$ (Carpenter and Morris) and $\bar{\alpha}_i = .1462 \times 10^{-3}$.

$\partial \bar{\alpha} / \partial b (mm)$	$+.14149130 \times 10^{-3}$
$\partial \bar{\alpha} / \partial \rho_m (kg/m^3)$	$+.23184345 \times 10^{-7}$
$\partial \bar{\alpha} / \partial B (Nmm)$	$-.24979009 \times 10^{-5}$
$\partial \bar{\alpha} / \partial E (N/mm^2)$	$-.14693146 \times 10^{-4}$
$\partial \bar{\alpha} / \partial K (N/mm^3)$	$-.21739922 \times 10^{-2}$

values. In theory, the stabilization of one class of instability leads to a destabilization of the other class. From the results at present, a means has been developed to measure the relative stabilizing-destabilizing effect of the two classes of instabilities. This is significant since it indicates the dominant influence of TSI waves in reference to the choice of compliant surface properties. So the optimization should be concerned with the stabilization of the more critical TSI waves.

From this comparison, a multi-variable algorithm is sought to minimize the TSI growth rate. Such an algorithm was made available by Dr. William Hagar of the Mathematics Department at Penn State. The algorithm is based on the conjugate gradient method by Fletcher and Reeves [43]. The code routinely calls the surface properties, gradients, and least damped wavenumber during the iterations. Beginning with the properties of Carpenter and Morris for $\theta = 60$, iterations are performed and listed in Table (6.2). For three iterations a stabilization begins to occur. This trend would continue and lead to a damped wavenumber. For each iteration a systematic repetition of property values is observed. This may occur due to the relative invariance of the sensitivity values. In using this algorithm the properties must have comparable magnitudes or the iterative process leads to physically unrealizable values. For example, the flexural rigidity which has a small magnitude was varied and became negative. This may be avoided by limiting the band of possible property values available to the algorithm. This is unnecessary at present since it proves more efficient computationally to use a simple variational approach. Although exact cpu accounts are unavailable, a relative comparison is possible. The above method requires approximately five minutes on the VAX 11/8580 as opposed to four minutes for the approach that will follow. The above method did confirm that stabilization is theoretically possible through the appropriate surface property combinations, but much more useful information is obtained from the

Table 6.2: Minimization of instability growth rate by the conjugate gradient approach for $B(Nm)=0.773 \times 10^{-7}$, $\rho_m(kg/m^3)=1000$, and an initial step of 0.05.

Iteration	b (mm)	E (N/mm ²)	K (N/mm ³)	$\bar{\alpha}_i$
Initial	.11100	.50900	.05900	-.003133
1	.10836	.50835	.05559	-.002791
	.10953	.50864	.05740	-.002946
	.10836	.50835	.05559	-.002791
2	.10716	.50806	.05402	-.002622
	.10769	.50819	.05472	-.002698
	.10716	.50806	.05402	-.002622
3	.10679	.50797	.05351	-.002567
	.10695	.50801	.05373	-.002592
	.10679	.50797	.05351	-.002567

method that will follow.

6.3 Variational Method and Results

For multi-variable problems it is advantageous to fix some variables. The characteristics of the remaining variables in the problem may then be observed. In the present discussion the flexural rigidity, thickness, and modulus of elasticity of the plate are functionally related, so the remaining parameters are fixed. This naturally occurs for the plate density since the sensitivity measurements in Table (5.2) show that the instability is not influenced significantly by density changes.

In this analysis a simple variation of properties is made. The properties are governed by the following relation

$$B = \frac{Eb^3}{12(1 - \nu^2)}, \quad (6.1)$$

where the Poisson's ratio, ν , is 0.5. Two approaches were used. The first approach maintains an essentially constant value of the flexural rigidity and appropriately varies the thickness and modulus of elasticity of the plate. The results are given in Table (6.3) and plotted in Figures (6.1) and (6.2) against the least damped wave-number of TSI. The results indicate that by simultaneously increasing the plate thickness and decreasing the modulus of elasticity a stabilization of the boundary layer may be realized. The second approach maintains essentially constant values of the thickness and modulus of elasticity and varies the flexural rigidity. These results are given in Table (6.4) and plotted in Figures (6.3) and (6.4). These results indicate that by decreasing the flexural rigidity the boundary layer tends to become stabilized. The most pronounced stabilization occurs when the plate thickness is increased and the modulus of elasticity is decreased. In both cases the FISI values show little change. This may be expected as indicated by the sensitivity

Table 6.3: Sensitivity of least stable wavenumber of TSI and FISI to changes the surface properties: B,E, and b with $K(N/mm^3)=.059$ and $\rho_m(kg/m^3) = 1000$.

B (Nm)	b (mm)	E (N/mm ²)	TSI $\bar{\alpha}_i$	FISI $\bar{\alpha}_i$
.743x10 ⁻⁷	.1035	.6031	-.3731x10 ⁻²	.1443x10 ⁻³
.743x10 ⁻⁷	.1085	.5235	-.3177x10 ⁻²	.1458x10 ⁻³
.743x10 ⁻⁷	.1135	.4573	-.2637x10 ⁻²	.1472x10 ⁻³
.743x10 ⁻⁷	.1185	.4019	-.2182x10 ⁻²	.1486x10 ⁻³
.743x10 ⁻⁷	.1235	.3550	-.1699x10 ⁻²	.1500x10 ⁻³
.763x10 ⁻⁷	.1285	.3236	-.1332x10 ⁻²	.1512x10 ⁻³
.763x10 ⁻⁷	.1335	.2886	-.0909x10 ⁻²	.1526x10 ⁻³
.763x10 ⁻⁷	.1385	.2585	-.0495x10 ⁻²	.1540x10 ⁻³
.763x10 ⁻⁷	.1435	.2324	-.0106x10 ⁻²	.1553x10 ⁻³
.763x10 ⁻⁷	.1485	.2097	+.0253x10 ⁻²	.1567x10 ⁻³
.783x10 ⁻⁷	.1535	.1948	+.0496x10 ⁻²	.1579x10 ⁻³
.783x10 ⁻⁷	.1585	.1770	+.0786x10 ⁻²	.1592x10 ⁻³
.783x10 ⁻⁷	.1635	.1612	+.1058x10 ⁻²	.1606x10 ⁻³
.783x10 ⁻⁷	.1685	.1473	+.1305x10 ⁻²	.1620x10 ⁻³
.783x10 ⁻⁷	.1735	.1349	+.1526x10 ⁻²	.1633x10 ⁻³
.803x10 ⁻⁷	.1785	.1271	+.1664x10 ⁻²	.1647x10 ⁻³
.803x10 ⁻⁷	.1835	.1170	+.1841x10 ⁻²	.1661x10 ⁻³
.803x10 ⁻⁷	.1885	.1079	+.2002x10 ⁻²	.1675x10 ⁻³
.803x10 ⁻⁷	.1935	.0997	+.2144x10 ⁻²	.1690x10 ⁻³
.803x10 ⁻⁷	.1985	.0924	+.2269x10 ⁻²	.1705x10 ⁻³
.823x10 ⁻⁷	.2035	.0879	+.2344x10 ⁻²	.1719x10 ⁻³
.823x10 ⁻⁷	.2085	.0817	+.2448x10 ⁻²	.1734x10 ⁻³
.823x10 ⁻⁷	.2135	.0761	+.2539x10 ⁻²	.1749x10 ⁻³
.823x10 ⁻⁷	.2185	.0710	+.2618x10 ⁻²	.1765x10 ⁻³
.823x10 ⁻⁷	.2235	.0663	+.2688x10 ⁻²	.1781x10 ⁻³

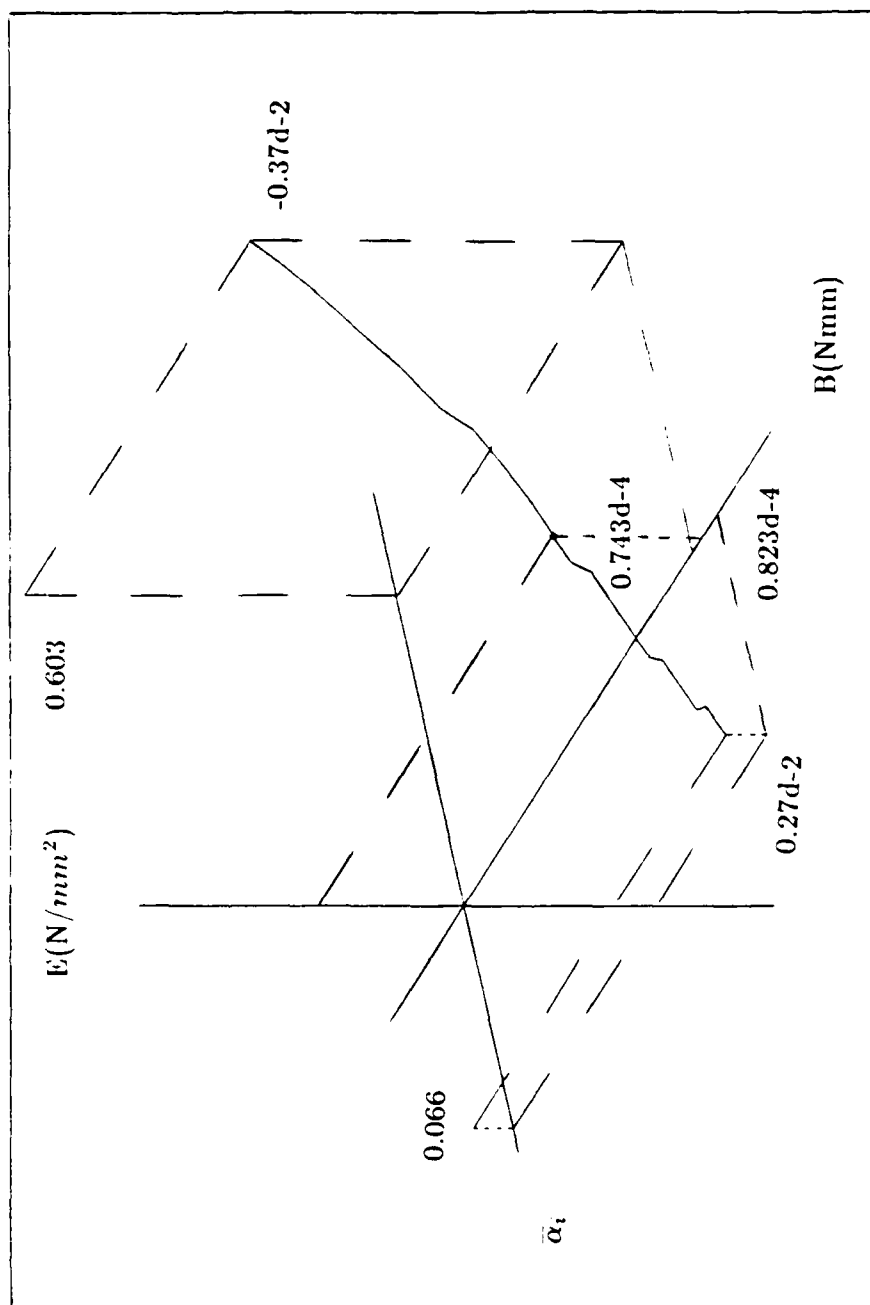


Figure 6.1: Variation of the least stable wavenumber for Tollmien-Schlichting instability versus B and E where E is primarily changed.

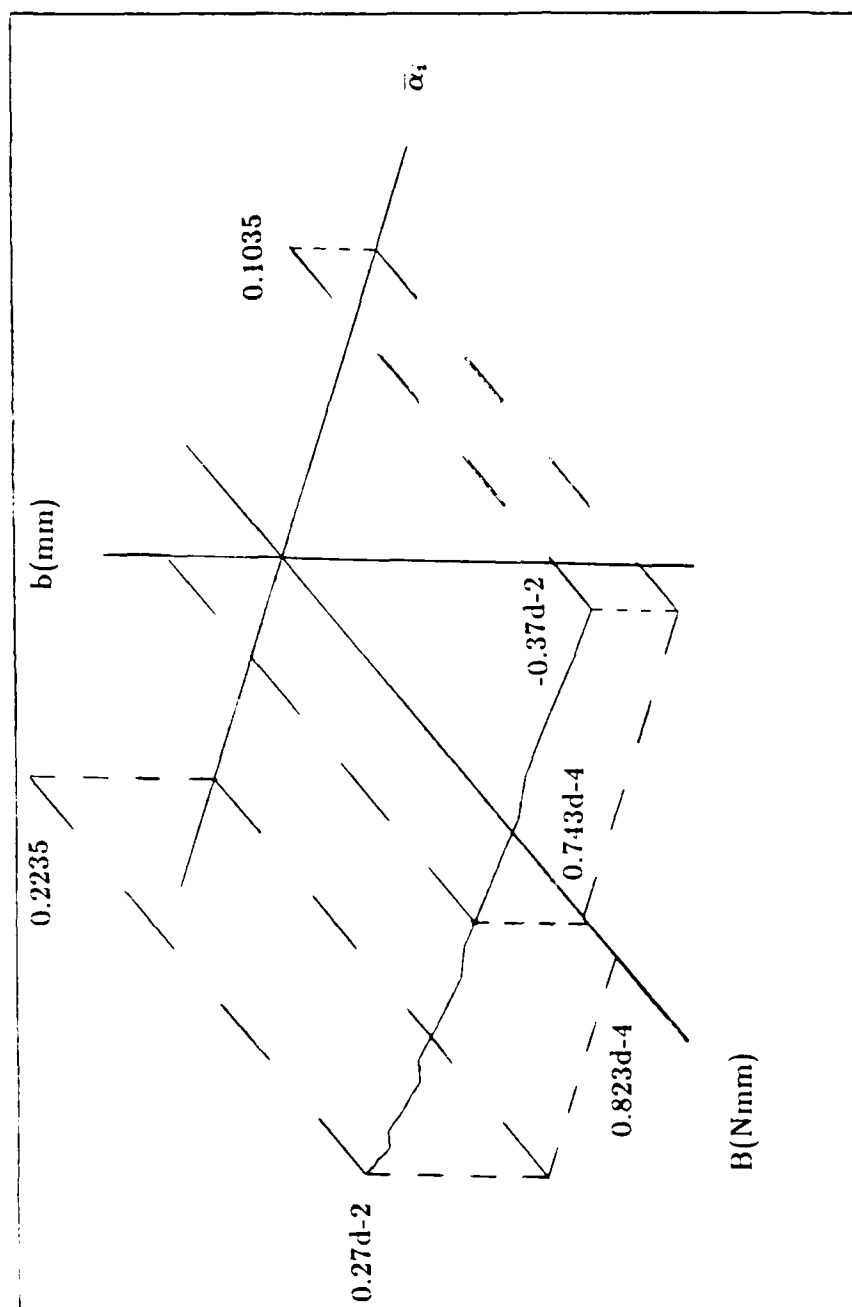


Figure 6.2: Variation of the least stable wavenumber for Tollmien-Schlichting instability versus B and b where b is primarily changed.

Table 6.4: Sensitivity of least stable wave-number of TSI and FISI to changes the surface properties: B,E, and b with $K(N/mm^3)=.059$ and $\rho_m(kg/m^3) = 1000$.

B (Nm)	b (mm)	E (N/mm ²)	TSI $\bar{\alpha}_i$	FISI $\bar{\alpha}_i$
.0743x10 ⁻⁶	.1035	.6031	-.3731x10 ⁻²	.1443x10 ⁻³
.0763x10 ⁻⁶	.1035	.6194	-.3878x10 ⁻²	.1441x10 ⁻³
.0783x10 ⁻⁶	.1035	.6356	-.4020x10 ⁻²	.1439x10 ⁻³
.0803x10 ⁻⁶	.1035	.6518	-.4158x10 ⁻²	.1437x10 ⁻³
.0823x10 ⁻⁶	.1035	.6681	-.4289x10 ⁻²	.1435x10 ⁻³
.0843x10 ⁻⁶	.1085	.5940	-.3917x10 ⁻²	.1448x10 ⁻³
.0863x10 ⁻⁶	.1085	.6081	-.4014x10 ⁻²	.1446x10 ⁻³
.0883x10 ⁻⁶	.1085	.6222	-.4139x10 ⁻²	.1445x10 ⁻³
.0903x10 ⁻⁶	.1085	.6363	-.4262x10 ⁻²	.1443x10 ⁻³
.0923x10 ⁻⁶	.1085	.6504	-.4381x10 ⁻²	.1441x10 ⁻³
.0943x10 ⁻⁶	.1135	.5805	-.4016x10 ⁻²	.1455x10 ⁻³
.0963x10 ⁻⁶	.1135	.5928	-.4102x10 ⁻²	.1453x10 ⁻³
.0983x10 ⁻⁶	.1135	.6051	-.4214x10 ⁻²	.1452x10 ⁻³
.1003x10 ⁻⁶	.1135	.6174	-.4324x10 ⁻²	.1450x10 ⁻³
.1023x10 ⁻⁶	.1135	.6297	-.4431x10 ⁻²	.1448x10 ⁻³
.1043x10 ⁻⁶	.1185	.5641	-.4074x10 ⁻²	.1462x10 ⁻³
.1063x10 ⁻⁶	.1185	.5749	-.4151x10 ⁻²	.1461x10 ⁻³
.1083x10 ⁻⁶	.1185	.5858	-.4253x10 ⁻²	.1459x10 ⁻³
.1103x10 ⁻⁶	.1185	.5966	-.4353x10 ⁻²	.1457x10 ⁻³
.1123x10 ⁻⁶	.1185	.6074	-.4451x10 ⁻²	.1456x10 ⁻³
.1143x10 ⁻⁶	.1235	.5461	-.4101x10 ⁻²	.1470x10 ⁻³
.1163x10 ⁻⁶	.1235	.5557	-.4171x10 ⁻²	.1468x10 ⁻³
.1183x10 ⁻⁶	.1235	.5652	-.4265x10 ⁻²	.1467x10 ⁻³
.1203x10 ⁻⁶	.1235	.5748	-.4357x10 ⁻²	.1465x10 ⁻³
.1223x10 ⁻⁶	.1235	.5843	-.4448x10 ⁻²	.1464x10 ⁻³

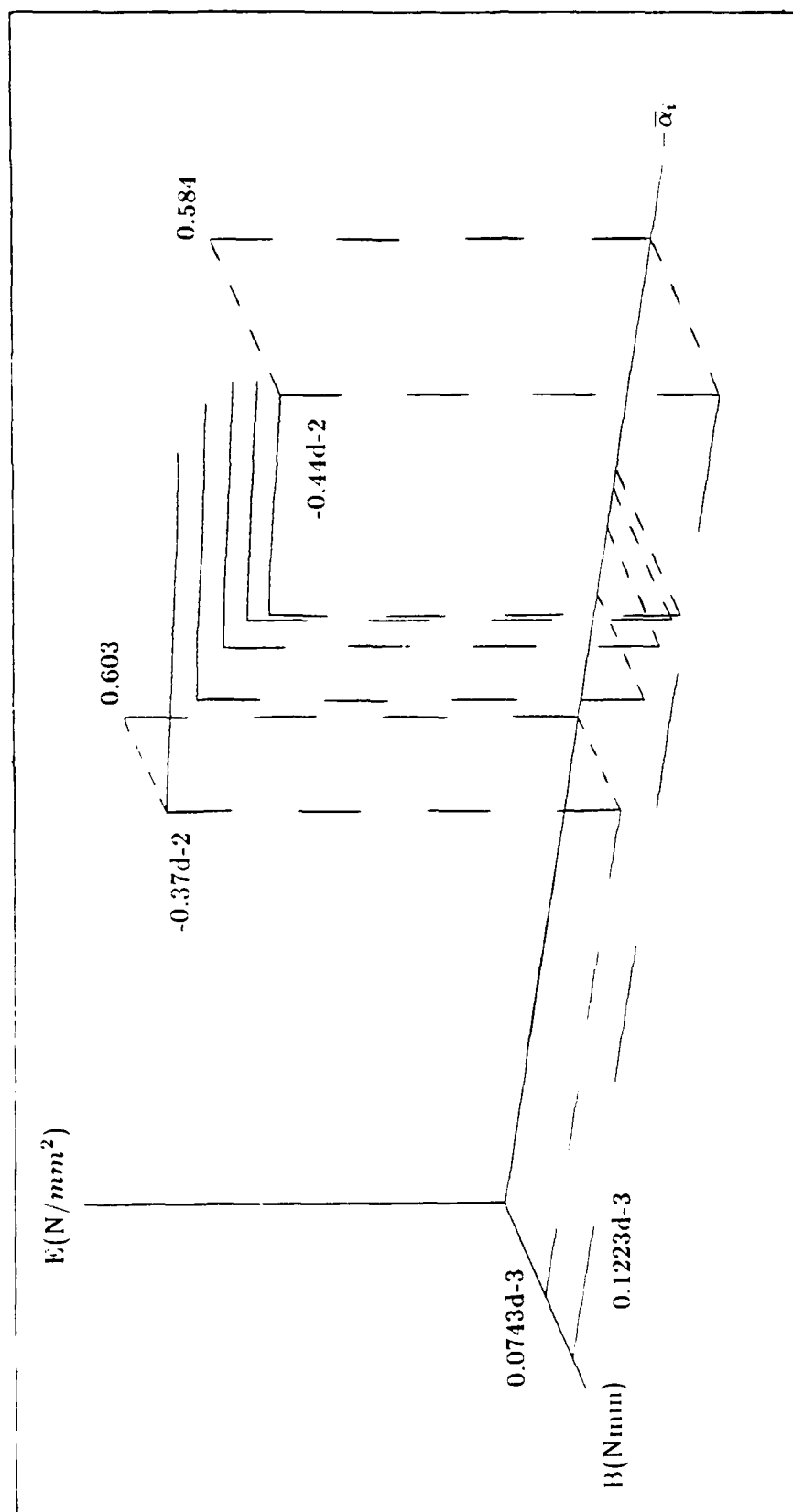


Figure 6.3: Variation of the least stable wavenumber for Tollmien-Schlichting instability versus B and E where B is primarily changed.

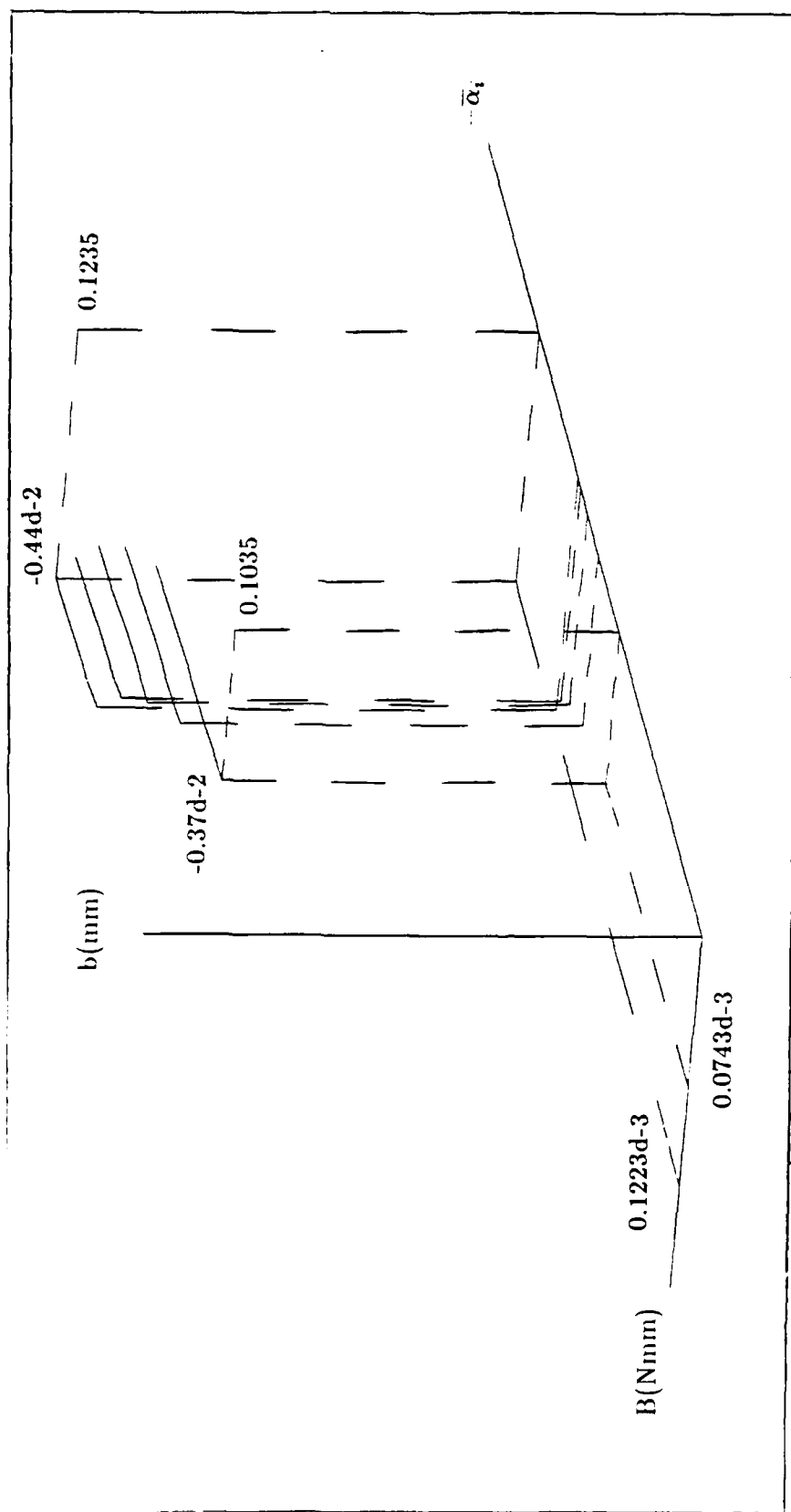


Figure 3.4: Variation of the least stable wavenumber for Tollmien-Schlichting instability versus B and b where B is primarily changed.

measurements. A more indepth explanation may be desired to justify that the results obtained with respect to FISI growth rate invariation are in agreement with theory. Carpenter and Garrad [18] developed a means to identify curves indicating expected stable and unstable regions for FISI. These curves are dependent on the properties of an isotropic surface for the temporal case. If their analysis were extended to the spatial non-isotropic case, it seems reasonable to expect that "stability curves" may be determined. The property variation in the present analysis may ensure that FISI remains in a neutral or stable region. It may be found that the destabilization of FISI waves occurring due to an increase in the plate thickness may be offset by the corresponding stabilization occurring due to an increase in the flexural rigidity.

The final variation is made with respect to the model swivel-arm angle. Shown in Figure (6.5) is the effect on the least damped wavenumber for TSI to changes in the swivel-arm angle for fixed surface properties. These properties correspond to those given by Carpenter and Morris for $\theta = 60$ with $R = 2240$ and $\bar{\omega} = 0.055$. As was found with the surface property changes, a stabilization may be realized. This can primarily be achieved with an angle between 0 and 50. It should be noted that the isotropic case corresponding to $\theta = 0$ has a stabilizing affect on the boundary layer for these particular surface properties, Reynolds number and frequency. This concludes the findings discovered through this investigation. Of course, further cases may be performed, but this example shows the relative importance of the surface properties on the instability and properties which may lead to a stabilization of the boundary layer.

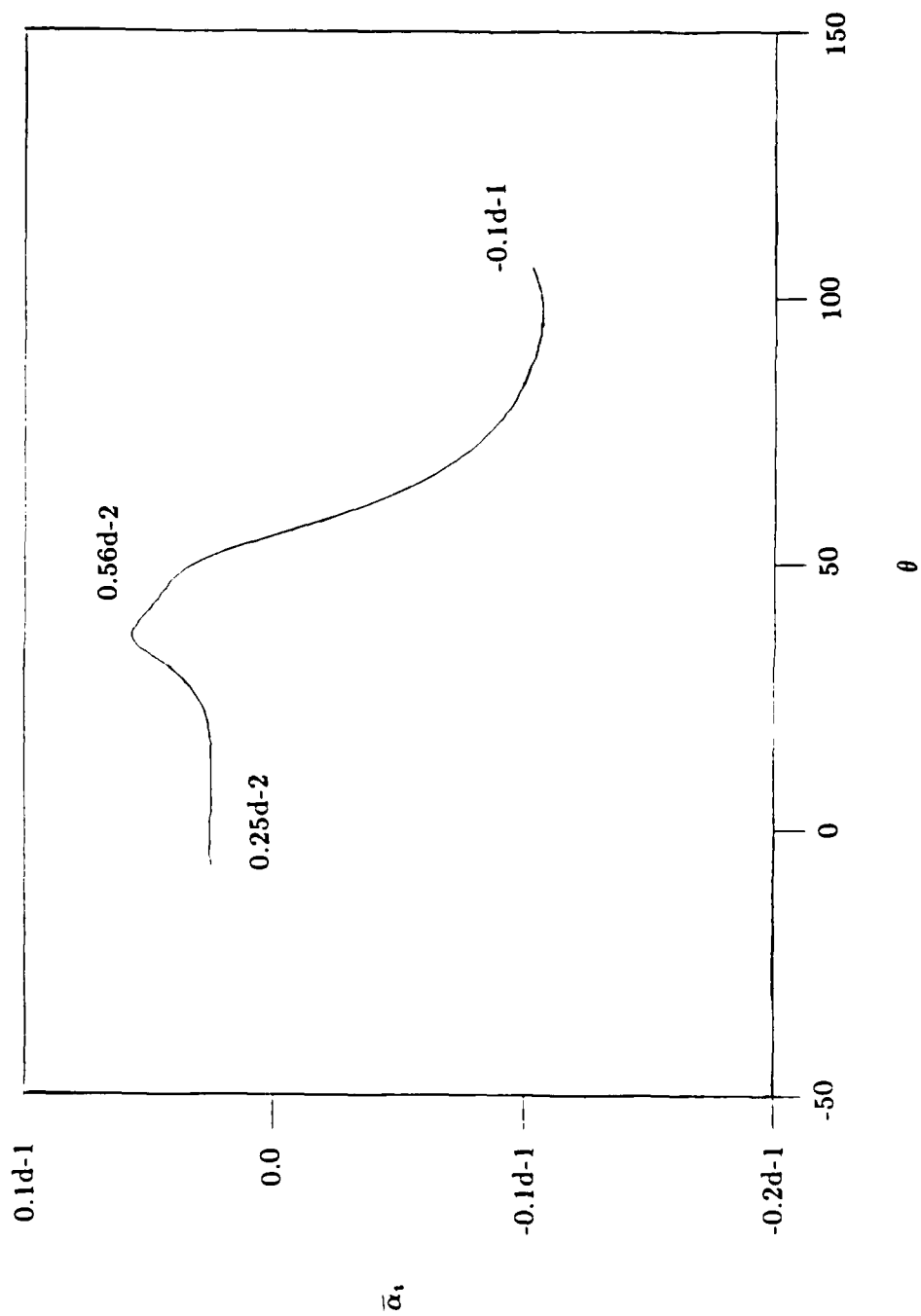


Figure 6.5: Variation of the least stable wave-number of Tollmien-Schlichting instability versus the swivel-arm angle, θ .

CHAPTER 7

DISCUSSION AND CONCLUSIONS

The majority of this thesis has consisted of a description of the problem and the building of the numerical tools necessary to fulfill the expectations of the investigation. The technique to determine the sensitivity of the instability with respect to surface property changes was critical in understanding the importance of each property. This measurement also provided a means to measure the relative influence of the surface properties on both TSI and FISI waves. The minimization algorithm seeks a decreasing gradient as a convergence criterion. In this analysis, however, the gradients changed very little over the property range of interest. So an algorithm which travels in a gradient dependent manner is less practical than a simple property variation for the present problem of interest. It also proves computationally more efficient and much more information is gained when the property variation approach is used. In extending the present analysis, the surface properties may be sought which give minimal sensitivity values. If this were attained, one might expect that with small changes in flow conditions the instability growth rate would essentially remain unchanged. The idea seems plausible but in fact the measure of sensitivity over the range of present property values did not change significantly in magnitude. This may be shown graphically by reviewing the slopes of the curves in Figures (6.1)-(6.4).

In the final method, the variation approach gives a simple means to attain stability curves with respect to surface properties. In a more complete sense, for a multi-variable problem it is possible to attain "stability planes". In this investigation the range of surface properties centered around the values by Carpenter and Morris. If manufacturable surface property combinations were available, it would

be possible to predict a coating most likely to delay transition. Assuming Kramer's conclusions concerning surface imperfections and water impurities resulting in no performance loss hold, the predicted performance should be realized if the manufactured compliant coating is in accord with the mechanical model representation.

From the results obtained in this investigation, further research may commence in many directions. Experimentally, a surface may be constructed and tested on a model. The performance may then be compared with an uncoated model and the predicted results of the mechanical model. Along a similar route taken in this study, the delay to transition may be analyzed for an optimal set of surface properties over a range of flow conditions. This is an obvious necessity for commercial considerations. Of course, compliant coatings are not limited to laminar transition analysis and are also being used in turbulence research. It would be of interest to determine the desirable compliant coating properties in turbulent flow. These properties could be compared with the "stability planes" which may be obtained from the present analysis. Overlap regions may be found which when used in practice delay transition and perform favorably after the transition to turbulent flow. This would enhance the performance of a coated vehicle over a range of velocities.

APPENDIX A

Chebyshev Series Formulae

The Chebyshev polynomials, $T_n(x)$, are defined on the interval $x \in [-1, +1]$ and are derived from and related to the cosine function by

$$T_n(\cos\theta) = \cos n\theta, \quad (\text{A.1})$$

with the initial few polynomials appearing as $T_0(x) = 1, T_1(x) = x$, $T_2(x) = 2x^2 - 1, T_3(x) = 4x^3 - 3x$, ect. The following trigonometric identity can be obtained.

$$\cos(n+1)\theta = 2\cos\theta \cdot \cos n\theta - \cos(n-1)\theta \quad (\text{A.2})$$

This results in a Chebyshev recurrence formula for higher order polynomials.

$$T_{n+1}(x) = 2xT_n(x) - T_{n-1}(x) \quad (\text{A.3})$$

The product formula is

$$T_n(x)T_m(x) = \frac{1}{2} (T_{n+m}(x) + T_{|n-m|}(x)) \quad (\text{A.4})$$

and the indefinite integral relation is

$$\int T_n(x)dx = \begin{cases} T_1(x) & n = 0 \\ \frac{1}{4} (T_0(x) + T_2(x)) & n = 1 \\ \frac{1}{2} \left[\frac{T_{n+1}(x)}{n+1} - \frac{T_{n-1}(x)}{n-1} \right] & n \geq 2. \end{cases} \quad (\text{A.5})$$

The series boundary conditions are

$$T_n(\pm 1) = (\pm 1)^n \quad (\text{A.6})$$

and the differential relation for Chebyshev polynomials at the boundaries is

$$\frac{d^p}{dx^p} T_n(\pm 1) = (\pm 1)^{n+p} \prod_{k=0}^{p-1} (n^2 - k^2) / (2k + 1). \quad (\text{A.7})$$

Another efficient relation useful when performing the summation of a Chebyshev series is given by

$$\sum_{n=0}^N {}'a_n T_n(x) = \frac{1}{2} [b_0(x) - b_{N+1}(x)], \quad (\text{A.8})$$

where the prime signifies that the leading term is to be halved. The recurrence system needed to evaluate (A.8) is

$$b_n(x) = 2xb_{n+1}(x) - b_{n+2}(x) + a_n \quad (\text{A.9})$$

$$b_{N+1}(x) = b_{N+2}(x) = 0.$$

A Chebyshev formula useful in approximating a known function in a Chebyshev series can be defined as

$$\Phi(x) = \sum_{n=0}^N {}'\phi_n T_n(x), \quad (\text{A.10a})$$

where $\Phi(x)$ is a known function at all points in the domain. The coefficients, ϕ_n , are given by

$$\phi_n = \frac{2}{N} \sum_{k=0}^N {}''\Phi(x_k) T_n(x_k) \quad (A.10b)$$

with

$$x_k = \cos \frac{k\pi}{N} \quad \text{for } k = 0, 1, 2, \dots, N. \quad (A.10c)$$

The double prime on the summation signifies that the leading and trailing coefficients are to be halved. The final Chebyshev property that will be given prior to listing practical integral formulae is the approximation of the differential of a known function in Chebyshev series. The derivative is given by

$$\phi'(x) = \sum_{n=0}^{\infty} b_n T_n(x) \quad (A.11a)$$

where

$$b_n = \frac{2}{c_n} \sum_{\substack{p=n+1 \\ p+n \text{ odd}}}^{\infty} p a_p \quad (A.11b)$$

and

$$c_n = \begin{cases} 2 & n = 0 \\ 1 & n > 0. \end{cases} \quad (A.11c)$$

The coefficients, a_n , are obtained from the series approximation to the known function, $\phi(x)$.

To obtain the solution of a differential equation by a Chebyshev series approximation, it is convenient, although not necessary, to convert the differential equation to an integral form. As such, a function is represented by the following finite, Chebyshev series.

$$\phi(x) = \sum_{n=0}^N ' a_n T_n(x) \quad (A.12)$$

By applying the integral relation (A.5) appropriately and repeatedly, the following relations are obtained.

$$1. \quad \int \phi(x) dx = \sum_{n=0}^{N+1} ' b_n T_n(x) \quad (A.13a)$$

where

$$b_n = \frac{1}{2n} (a_{n-1} - a_{n+1}) \quad \text{for } n \geq 1 \quad (A.13b)$$

$$2. \quad \int \int \phi(x) dx^2 = \sum_{n=0}^{N+2} ' b_n T_n(x) \quad (A.14a)$$

where

$$b_n = \left[\frac{a_{n-2}}{4n(n-1)} - \frac{a_n}{2(n^2-1)} + \frac{a_{n+2}}{4n(n+1)} \right] \quad \text{for } n \geq 2 \quad (A.14b)$$

$$3. \quad \int \int \int \phi(x) dx^3 = \sum_{n=0}^{N+3} ' b_n T_n(x) \quad (A.15a)$$

where

$$b_n = \frac{a_{n-3}}{8n(n-1)(n-2)} - \frac{3a_{n-1}}{8n(n-2)(n+1)} + \frac{3a_{n+1}}{8n(n-1)(n+2)} - \frac{a_{n+3}}{8n(n+1)(n+2)} \quad \text{for } n \geq 3 \quad (A.15b)$$

$$4. \quad \int \int \int \int \phi(x) dx^4 = \sum_{n=0}^{N+4} ' b_n T_n(x) \quad (A.16a)$$

where

$$b_n = \frac{a_{n-4}}{16n(n-1)(n-2)(n-3)} - \frac{a_{n-2}}{4n(n^2-1)(n-3)} + \frac{3a_n}{8(n^2-1)(n^2-4)} - \frac{a_{n+2}}{4n(n^2-1)(n+3)} + \frac{a_{n+4}}{16n(n+1)(n+2)(n+3)} \quad \text{for } n \geq 4 \quad (\text{A.16b})$$

When the coefficients in the differential equations are non-constant, the Chebyshev product formula (A.4) is needed. Introducing a function, $u(x)$, representing the non-constant coefficient, the following is obtained.

$$u(x)\phi(x) = \sum_{n=0}^{\infty} d_n T_n(x) \quad (\text{A.17a})$$

with

$$u(x) = \sum_{n=0}^{\infty} u_n T_n(x) \quad (\text{A.17b})$$

and

$$d_n = \frac{1}{2}u_n a_0 + \frac{1}{2} \sum_{m=1}^N (u_{|m-n|} + u_{m+n})a_m \quad \text{for } n \geq 0 \quad (\text{A.17c})$$

Integrations are performed in a straight forward manner using the integral relation (A.5). The following integral relations prove useful for the problem presented in this thesis.

$$1. \int u(x)\phi(x)dx = \sum_{n=0}^{N+1} d_n T_n(x) \quad (\text{A.18a})$$

where

$$d_n = \frac{1}{4n}(u_{n-1} - u_{n+1})a_0 + \frac{1}{4n} \sum_{m=1}^N (u_{|m-n+1|} - u_{|m-n-1|} - u_{m+n-1} - u_{m+n+1})a_m \quad \text{for } n \geq 1 \quad (\text{A.18b})$$

$$2. \int \int u(x) \phi(x) dx^2 = \sum_{n=0}^{N+2} ' d_n T_n(x) \quad (A.19a)$$

where

$$d_n = \left[\frac{u_{n-2}}{8n(n-1)} - \frac{u_n}{4(n^2-1)} + \frac{u_{n+2}}{8n(n+1)} \right] a_0 + \sum_{m=1}^N \left[\frac{u_{|m-n+2|} + u_{m+n-2}}{8n(n-1)} - \frac{u_{m+n} + u_{|m-n|}}{4(n^2-1)} + \frac{u_{|m-n-2|} + u_{m+n+2}}{8n(n+1)} \right] a_m \quad \text{for } n \geq 2 \quad (A.19a)$$

$$3. \int \int \int u(x) \phi(x) dx^3 = \sum_{n=0}^{N+3} ' d_n T_n(x) \quad (A.20a)$$

where

$$d_n = \left[\frac{u_{n-3}}{16n(n-1)(n-2)} - \frac{3u_{n-1}}{16n(n+1)(n-2)} + \frac{3u_{n+1}}{16n(n-1)(n+2)} - \frac{u_{n+3}}{16n(n+1)(n+2)} \right] a_0 + \sum_{m=1}^N \left[\frac{u_{|m-n+3|} + u_{m+n-3}}{16n(n-1)(n-2)} - \frac{3(u_{|m-n+1|} + u_{m+n-1})}{16n(n+1)(n-2)} + \frac{3(u_{|m-n-1|} + u_{m+n+1})}{16n(n-1)(n+2)} - \frac{u_{|m-n-3|} + u_{m+n+3}}{16n(n+1)(n-2)} \right] a_m \quad \text{for } n \geq 3 \quad (A.20b)$$

$$4. \int \int \int \int u(x) \phi(x) dx^4 = \sum_{n=0}^{N+4} ' d_n T_n(x) \quad (A.21a)$$

where

$$d_n = \left[\frac{u_{n-4}}{32n(n-1)(n-2)(n-3)} - \frac{u_{n-2}}{8n(n^2-1)(n-3)} + \frac{3u_n}{16(n^2-1)(n^2-4)} - \frac{u_{n+2}}{8n(n^2-1)(n+3)} + \frac{u_{n+4}}{32n(n+1)(n+2)(n+3)} \right] a_0 + \sum_{m=1}^N \left[\frac{u_{|m-n+4|} + u_{m+n-4}}{32n(n-1)(n-2)(n-3)} - \frac{u_{|m-n+2|} + u_{m+n-2}}{8n(n^2-1)(n-3)} - \frac{3(u_{|m-n|} + u_{m+n})}{16(n^2-1)(n^2-4)} + \frac{u_{|m-n-2|} + u_{m+n+2}}{8n(n^2-1)(n+3)} - \frac{u_{|m-n-4|} + u_{m+n+4}}{32n(n+1)(n+2)(n+3)} \right] a_m \quad \text{for } n \geq 4 \quad (A.21b)$$

These integral relations replace the appropriate integral terms in an integral equation in order to obtain a solution. The integral formulae require the order of the Chebyshev terms to begin with the order of the integral equation. The proof of this will not be given here, but can be found in [31].

APPENDIX B

BLASIUS SOLUTIONREPRESENTED BY A CHEBYSHEV SERIES

In this thesis, the solution to the Blasius equation is necessary and is represented by a Chebyshev series. In order to attain this end, an accurate means of obtaining a numerical solution is first necessary. In the similarity variables the governing equation is an ordinary differential equation of the form

$$f''' + \frac{1}{2} f f'' = 0 \quad (B.1)$$

where $(') = \frac{d}{d\eta}$ and the appropriate boundary conditions are

$$f(0) = f'(0) = 0 \quad , \quad \lim_{\eta \rightarrow \infty} f'(\eta) \rightarrow 1. \quad (B.2)$$

where the derivative of $f(\eta)$ is the streamwise velocity. Using a shooting-type method with a 5th-6th order, variable-step Runge-Kutta solver(IMSL:DVERK) , the initial condition satisfying the streamwise velocity limit can be found. This results in

$$f''(0) = 0.3320573362185815 . \quad (B.3)$$

The discrete points desired in the Chebyshev domain, $z \in [-1, +1]$, are transformed to the Blasius variable, $\eta \in [0, \infty)$, via the algebraic transformation

$$\eta = L \cdot (1 + y) / (1 - y) \quad (B.4)$$

with

$$y = \hat{y} Re_x^{-\frac{1}{2}} \quad (B.5)$$

where \hat{y} is the physical coordinate with domain $[0, \infty)$. The solution obtained at the desired points are then transformed back to the computational domain using the inverse of (B.4). Taking the solution of a function (i.e., the Blasius solution), $F(z)$, given at all points in $z \in [-1, +1]$, a Chebyshev expansion of such is sought.

$$F(z) = \sum_{n=0}^N ' f_n T_n(z) \quad (B.6)$$

The prime signifies that the leading term of the series is to be halved. An exact solution is obtained for $N \rightarrow \infty$. For a series expansion, the function must be evaluated at the Chebyshev points

$$z_i = \cos(\pi i/N) \quad i = 0, 1, 2, \dots, N. \quad (B.7)$$

The series at these points is

$$F(z_i) = \sum_{n=0}^N ' f_n T_n(z_i). \quad (B.8)$$

Using the relationship between the Chebyshev polynomial and the cosine function, a curve-fitting formula can be obtained. Thus, the coefficients can be computed using

$$f_n = \frac{2}{N} \sum_{i=0}^N '' f(z_i) T_n(z_i)$$

AD-A198 433

THE SENSITIVITY OF BOUNDARY LAYER INSTABILITY GROWTH
RATES TO COMPLIANT M. (U) PENNSYLVANIA STATE UNIV
UNIVERSITY PARK APPLIED RESEARCH LAB.

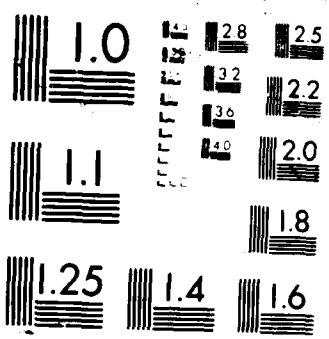
2/2

UNCLASSIFIED

R D JOSLIN ET AL. DEC 87 ARL/PSU/TR-87-014 F/G 20/4

NL





where the double prime signifies that the leading and trailing terms of the series are to be halved. With the identity

$$T_n(z_i) = \cos(\pi ni/N) \quad (B.10)$$

the desired form of the curve-fitting formula is obtained. Making a substitution of (B.10) into (B.9), the following results

$$f_n = \frac{2}{N} \sum_{i=0}^N {}''f(z_i) \cos(\pi ni/N) . \quad (B.11)$$

By making use of (B.11) with (B.6), the Chebyshev series representation of a function can be computed to a desired accuracy by taking N to be large.

The solution of the Blasius equation represented by a Chebyshev series is attained with this curve-fitting formula. Sufficient accuracy was attained using an approximation with an order of $N = 99$. The solution given in the computational domain is shown in Figure (3.1) in Chapter 3.

REFERENCES

- [1] Kramer M.O., "Boundary layer stabilization by distributed damping," *ASNE Journal*, February 1960, pp. 25-33.
- [2] Kramer M.O., "Boundary layer stabilization by distributed damping," *ASNE Journal: Reader's Forum*, February 1960.
- [3] Benjamin T.B., "Effects of a flexible boundary on hydrodynamic stability," *J. Fluid Mech.*, **9**, (1960), pp. 513-532.
- [4] Lin C.C., "On the stability of two-dimensional parallel flows. Part 1.—General theory," *Quart. Appl. Math.*, **3**, (1946), pp. 117-142.
- [5] Lin C.C., "Part 2.—Stability in an inviscid fluid," *Quart. Appl. Math.*, **3**, (1946), pp. 218-234.
- [6] Lin C.C., "Part 3.—Stability in a viscous fluid," *Quart. Appl. Math.*, **3**, (1946), pp. 277-301.
- [7] Miles J.W., "On the generation of surface waves by shear flows." *J. Fluid Mech.*, **3**, (1957), pp. 185-204.
- [8] Miles J.W., "On the generation of surface waves by shear flows. Part 2," *J. Fluid Mech.*, **5**, (1959), pp. 568-582.
- [9] Miles J.W., "On the generation of surface waves by shear flows. Part 3," *J. Fluid Mech.*, **5**, (1959), pp. 583-598.
- [10] Miles J.W., "On the generation of surface waves by shear flows. Part 4," *J. Fluid Mech.*, **7**, (1961), pp. 433-448.
- [11] Landahl M.T., "On the stability of a laminar incompressible boundary layer over a flexible surface," *J. Fluid Mech.*, **13**, (1962), pp. 609-632.
- [12] Benjamin T.B., "The three-fold classification of unstable disturbances in flexible surface bounding inviscid flows." *J. Fluid Mech.*, **16**, (1963), pp. 436-450.

- [13] Benjamin T.B., "Fluid flow with flexible boundaries," *Proc. 11th Int. Cong. of Applied Mech.*, Munich, (1964), pp. 109-128.
- [14] Grosch C.E. and Salwen H., "The continuous spectrum of the Orr-Sommerfeld equation: Part 1. The spectrum and the eigenfunction," *J. Fluid Mech.*, **87**(1), (1978), pp. 33-54.
- [15] Grosskreutz R., "Wechselwirkungen zwischen turbulenten Grenzschichten und weichen Wander," MPI fur Stromungsforschung und der AVA, Gottingen, Mitt. No. 53, (1971).
- [16] Grosskreutz R., "An attempt to control boundary layer turbulence with non-isotropic compliant walls," *University Science Journal*, (Dares Salaam Univ.), **1**(1), (1975), pp. 65-73.
- [17] Carpenter P.W. and Garrad A.D., "The hydrodynamic stability of flow over Kramer-type compliant surfaces: Part 1. Tollmien-Schlichting instabilities," *J. Fluid Mech.*, **155**, (1985), pp. 465-510.
- [18] Carpenter P.W. and Garrad A.D., "The hydrodynamic stability of flow over Kramer-type compliant surfaces: Part 2. Flow-induced surface instabilities," *J. Fluid Mech.*, **170**, (1986), pp. 199-232.
- [19] Carpenter P.W. Gaster M. and Willis G.J.K., "A numerical investigation into boundary layer stability on compliant surfaces," **Numerical Methods in Laminar and Turbulent Flow**, (ed. C. Taylor et al.), (1983), pp. 166-172.
- [20] Carpenter P.W., "The optimization of compliant surfaces for transition delay," Technical note 85/2, October 1985, University of Exeter, U.K.
- [21] Carpenter P.W., "The optimization of compliant surfaces for transition delay," *Proc. IUTAM Symp. on Turbulence Management and Relaminarization*, 19-23 January 1987/Bangalore, India.

- [22] Carpenter P.W., "Transition to turbulence in boundary layers on compliant surfaces," Progress report for the second six months(April-Sept. 1984), January 1985, University of Exeter, U.K.
- [23] Carpenter P.W. and Morris P.J., "The hydrodynamic stability of flows over non-isotropic compliant surfaces-numerical solution of the differential eigenvalue problem," **Numerical Methods in Laminar and Turbulent Flow**, (ed. C. Taylor et al.), (1985), pp. 1613-1620.
- [24] Carpenter P.W., "The hydrodynamic stability of flows over simple non-isotropic compliant surfaces," *Proc. Int. Conf. on Fluid Mech.*, 1-4 July 1987/Beijing, China.
- [25] Morris P.J., "Applications of matrix factorization in hydrodynamic stability," *4th Army Conference on Applied Mathematics and Computing*, 27-30 May 1987/Cornell.
- [26] Squire H.B., "On the stability of three-dimensional disturbances of viscous fluid flow between parallel walls," *Proc. Roy. Soc. London(A)*, **142**, (1933), pp. 621-628.
- [27] Bridges T.J. and Morris P.J., "Spectral calculations of the spatial stability of non-parallel boundary layers," *AIAA 22nd Aerospace Science Meetings*, 9-12 January 1984/Reno, Nevada (AIAA-84-0437).
- [28] Bridges T.J. and Morris P.J., "A note on boundary layer stability calculations," (accepted for publication) *Phys. Fluids*, (1987).
- [29] Bridges T.J., "A mathematical analysis of the effect of freestream turbulence on the Blasius boundary layer," Ph.D. Thesis, (1984), Department of Aerospace Engineering, The Pennsylvania State University.
- [30] Grosch C.E. and Orszag S.A., "Numerical solution of problems in unbounded regions: coordinate transforms," *J. Comput. Phys.*, **25**, (1977), pp. 273-296.

- [31] Gottlieb D. and Orszag S.A., **Numerical Analysis of Spectral Methods: Theory and Applications**, SIAM **26**, Philadelphia, PA. (1986).
- [32] Fox L. and Parker I.B., **Chebyshev Polynomials in Numerical Analysis**, Oxford University Press, (1968).
- [33] Bridges T.J. and Morris P.J., "Differential eigenvalue problems in which the parameter appears nonlinearly," *J. Comput. Phys.*, **55** (3), (1984), pp. 437-460.
- [34] Lancaster P., "Algorithms for lambda-matrices," *Numerische Mathematik*, **6**, (1964), pp. 388-394.
- [35] Benney D.J. and Orszag S.A., "Stability analysis for laminar flow control. Part I," NASA CR-2910, (1977).
- [36] Gohberg I. Lancaster P. and Rodman L., **Matrix Polynomials**, Computer Science and Applied Mathematics, Academic Press, (1982).
- [37] Dennis J.E. Jr. Traub J.F. and Weber R.P., "Algorithms for solvents of matrix polynomials," *SIAM J. Numer. Anal.*, **15**(3), (1978), pp. 523-533.
- [38] Traub J.F., "A class of globally convergent iteration functions for the solution of polynomial equations," *Math. Comput.*, **20**, (1966), pp. 113-138.
- [39] Jordinson R., "The flat plate boundary layer. Part 1. Numerical integration of the Orr-Sommerfeld equation," *J. Fluid Mech.*, **43**(4), (1970), pp. 801-811.
- [40] Van Stijn Th.L and Van De Vooren A.I., "An accurate method for solving the Orr-Sommerfeld equation," *Journal of Engineering Math.*, **14**, (1980), pp. 17-26.
- [41] Gere J.M. and Timoshenko S.P., **Mechanics of Materials**, 2nd Ed., Brooks/Cole Engineering Division, Monterey/California, (1984).

- [42] Powell M.J.D., "An efficient method for finding the minimum of a function of several variables without calculating derivatives," *The Computer Journal*, **7**, (1964), pp. 155-162.
- [43] Fletcher R. and Reeves C.M., "Function minimization by conjugate gradients," *The Computer Journal*, **7**, (1964), pp. 149-154.

END
DATE
FILMED

4-88

DTIC